MATHEMATICAL, PHYSICAL, AND ENGINEERING SCIENCES DIVISION

AN ANTIMICROBIAL TRITERPENE FROM THE LEAVES OF *Lantana camara* L. (FAM. VERBENACEAE)

JUANITA BARRE[1], GERARDO C. JANAIRO[2], and CONSOLACION RAGASA[2]

[1]*College of Science and Mathematics*
Western Mindanao State University
7000 Zamboanga City

[2]*De La Salle University*
Taft Avenue, Malate, 0922 Manila

ABSTRACT

Lantana camara L. leaves afforded a novel triterpene 22β-acetoyloxylantic acid (**1**), 22β-dimethylacryloyloxylantanolic acid (**2**), a mixture of 22β-dimethylacryloyloxylantanolic acid (**2**) and 22β-angeloyloxylantanolic acid (**3**), lantanolic acid (**4**), and lantic aid (**5**) by gravity column chromatography (dry packing). The structure of **1** was elucidated by NMR and FT-IR spectroscopy and mass spectrometry, while the structures of **2-5** were elucidated by comparison of their ^{1}H NMR spectral data with those of **1**. Compound **1** was tested for its antimicrobial potential against six microorganisms and was found active against *Staphylococus aureus* and *Salmonella typhi*. It was also tested for its anti mutagenicity potential by the micronucleus test. Results of the study indicated that it reduced the number of micronucleated polychromatic erythrocytes by 76.7% at a concentration of 6.75 mg/kg mouse.

KEY WORDS: *Lantaca camara*, Verbenaceae, triterpenes, lantanolic acid, antimicrobial

INTRODUCTION

Lantana camara L. is a native of tropical America, but now occurs throughout the Philippines in thickets and waste lands at low and medium altitudes [1]. Crushed leaves of *L. camara* are applied as poultice to wounds and injuries, while

the decoction of boiled leaves is used for washing affected areas in cases of dermatitis, eczema, tinea, and furuncles. Antipyretic properties of the leaves are mainly attributed to lantadene A [2]. Previous investigations of *L. camara* afforded triterpenes of the lantadene type [3-6], lantanolic acid [3], lantic acid [4], icterogenin and hederagonic acid [7], camaroside and phenolic compounds [8]. We now report the isolation of a new triterpene (**1**) and its antimicrobial and antimutagenic properties.

EXPERIMENTAL

General Experimental Procedures

NMR spectra were recorded in $CDCl_3$ solutions on a Brucker AM 300 NMR spectrometer with $CDCl_3$ (7.26, 77.0 ppm) as reference. Eims were carried out on a JEOL D 100 mass spectrometer. Si gel type 60 (Merck) was used for column chromatography and plastic-backed plates coated with Si gel F254 (Merck) for thin layer chromatography. Plates were visualized by spraying with vanillin/H_2SO_4 and warming.

Biological Material

Leaves of the pink-flowered variety of *Lantana camara* were collected from the University of the Philippines Los Baños campus in March 1994.

Extraction and Isolation

The air-dried leaves (600 g) were soaked in $CHCl_3$ (3.6 L) for the three days to afford a crude extract (23 g). The extract (4 g) was chromatographed on a gravity column packed with dry silica gel (70-230 mesh) using increasing proportions of acetone in $CHCl_3$ (5% increment) and CH_3OH in acetone (10% increment) as eluents. The 30-50% methanol in acetone fractions were rechromatographed in 7:1.5:1.5 (DCM:Et_2O:acetonitrile) as eluent to afford **1** [colorless crystals, m. pt. 270-273 °C, α_D = 87.72 ($CHCl_3$), 30 mg]. The 10-20% acetone in $CHCl_3$ fractions were rechromatographed in 10% $CHCl_3$ to afford **2** [colorless cystals, m. pt. 285-287 °C α_D = +115.38 °C ($CHCl_3$, 33 mg]. The 25.60% acetone in $CHCl_3$ fractions were rechromatographed in 15% acetone in $CHCl_3$ to afford **4** (colorless crystals, 21.7 mg) and a mixture of **2** and **3**.

Antimicrobial Test

A microbial suspension containing approximately 10^7 cells/mL was prepared for each test organism for 24-hour agar culture using 0.1% peptone water. One-tenth (0.1) mL of the bacterial suspension was transferred into a pre-poured 30 mL deep nutrient agar plate, the yeast suspension into a glucose yeast peptone agar plate, and the fungal suspension on a potato dextrose agar plate. About 5 mL of

the corresponding melted agar cooled to about 45°C was immediately poured into the plate. The plate was swirled to distribute the microbial cells evenly on the plate. After the overlay agar had solidified, three 1-cm diameter holes were cut from equidistant points using a sterile cork borer.

One-tenth (0.1) mL portions of the extract (30 μg/mL) were placed in duplicate holes per organism. Similar volumes of the solvent acetone and of the corresponding antibiotic for each test organism were placed in the remaining two wells on the plate. Plates were incubated at room temperature to prevent evaporation of liquid on the petri lid that may cause interference in distribution of organisms on the surface. Bacterial and yeast plates were read after 24 hours, while the mold plate was read after three days. Clearing zones were measured in millimeters (mm), the average for each supernatant was taken, and the antimicrobial activity index (AI) was computed.

Antimutagenicity Test

Mitomycin C (2.75 mg/kg mouse) dissolved in H_2O and **1** (6.75 mg/kg mouse) dissolved in DMSO (7.5 mL/kg mouse) was administered orally and simultaneously to mice of the Swiss strain (source: DOST). For the positive control, only mitomycin C (2.75 mg/kg mouse) and DMSO (7.5 mL/kg mouse) were administered orally to mice. Five mice each were tested for **1** and the positive control. The second administration was conducted after twenty-four hours. Six hours after the second treatment, the mice were sacrificed and blood from the bone marrow was flushed with fetal calf serum. Smears on slides, three per mouse were prepared, and were stained with undiluted May-Gruenwald, followed by 50% May-Gruenwald solution, then 15% Giemsa stain. The number of micronucleated polychromatic erythrocytes (MPCE) per 1,000 polychromatic erythrocytes was counted with the use of a high power microscope and the results are given as % reduction in MPCE.

RESULTS AND DISCUSSION

The chloroform extract of the air-dried leaves of *L. camara* (pink-flowered variety) afforded a novel triterpene (**1**), 22β-dimethylacryloyloxylantanolic acid (**2**), a mixture of **2** and 22β-angeloyloxylantanolic acid (**3**), lantanolic acid (**4**), and lantic acid (**5**). The structure of **1** was elicited by NMR (^1H, ^{13}C, DEPT, COSY) and FT-IR spectroscopy, and mass spectrometry, while the structures of **2-5** were elucidated by comparison of their ^1H NMR spectral data with that of **1**.

The ^1H NMR spectrum of **1** indicated an olefinic H at δ 5.40, a carbinyl H of an ester at δ 4.95, and carbinyl Hs of an ether or alcohol at δ 4.21 and δ 3.90. The ester functionality of **1** is confirmed by the FT-IR absorption band at 1250 cm^{-1} and 1720 cm^{-1}. The spectrum also indicated seven methyl groups, one of which belongs to an acetate at δ 2.00 (Table 1).

Table 1. Comparison of the ^1H NMR Spectral Data of **1-4**

Chemical Shifts, δ					Functionalities
1	2	3	4	5	
5.39	5.60, 5.39	5.39	5.29	5.29	C=CH
4.95	4.95	4.95			CH-O (ester)
4.21, 3.90	4.21, 3.90	4.21, 3.90	4.21, 3.90	4.21, 3.90	CH_2O
1.14(s), 1.08 (s), 1.01 (s), 0.95 ($2CH_3$, d), 0.78 (s)	1.18(s), 1.08(s), 1.04(s0, 1.08(s), 0.92(s0, 0.79(s)	1.25(s), 1.16(s), 1.04(s), 1.00(s), 0.90(s), 0.80(s)	1.38(s), 1.27(s), 1.05(s), 1.16(s), 0.96(s), 0.73(s)	1.14(s),1.08(s), 1.01(s), 0.95 ($2CH_3$,d), 0.98(s)	CH_2
2.00					$CH_3C=O$
	2.15(s,br), 1.88(s,br)				$CH_3)_2=C$
		6.00(m)			C=CH
		1.04($2CH_3$,d)			$CH_3C=CCH_3$

Further information was given by the ^{13}C and DEPT NMR spectra of **1**. The spectra indicated the following functionalities: a carbonyl of an ester at 170.2 ppm, a carbonyl of a carboxylic acid at 178.5 ppm (IR ν_{max} 3400 cm^{-1}), an acetal at 98.9 ppm (IRν_{max} 1020 cm^{-1}), an oxygenated methylene C at 67.9 ppm, an oxygenated methine C at 75.7 ppm, a fully substituted olfefinic C at 137.2 ppm, a methine olefinic C at 126.1 ppm, eight methylene Cs, and seven methyl Cs (Table 2). Thus, **1** contained thirty-two carbons, forty-eight hydrogens, and six oxygens. This was supported by the mass spectrum which showed a molecular ion peak at 528 (5%) which corresponds to a molecular formula of $C_{32}H_{48}O_6$. The peak at m/z 468 (40%)

Table 2. Comparison of ^{13}C NMR Spectra of **1-2**

2	1	Functionalities
178.0	178.5	COOH (acid)
163.4	170.2	C=O (ester)
143.0, 116.0	137.2	C=
157.0, 122.5	126.1	CH=
98.9	98.9	O-C-O
67.7	67.9	CH_2-O
75.3	75.7	CH-O
	49.3, 42.4, 41.9, 40.2, 39.2	C
	50.2, 49.3, 41.9, 39.2, 32.2	CH
	35.1, 34.9, 31.2, 29.8, 27.9, 24.8, 23.8, 19.6	CH_2
	16.9, 17.7, 18.4, 20.7, 21.2, 23.1, 27.1	CH_3

resulted from the loss of acetic acid, while the peak at m/z 450 (18%) resulted from the loss of acetic acid and H_2O. From the molecular formula, the index of hydrogen deficiency is nine. With three double bond equivalents (2 C=O and 1 C=C) deduced from the ^{13}C and DEPT NMR spectra of **1**, the remaining hydrogen deficiency can be attributed to six carbocyclic systems.

The COSY spectrum indicated the following isolated systems: a carbinyl H at δ 4.95 was coupled to the Hs at δ 1.47 and δ 1.79, with the latter coupled to the H at δ 1.35, which was in turn coupled to the methyl Hs at δ 0.92 and the H at δ1.38, with the latter coupled to the H at δ 1.52 and the methyl Hs at δ 0.92; an olefinic H at δ 5.35 was coupled to the allylic methylene Hs at δ 1.79 and δ 2.10, with the latter coupled to the H at δ 1.23; the H at δ 2.40 was coupled to the H at δ 1.78 and the methylene Hs at δ 1.35 and δ 0.84; the methylene Hs at δ 2.14 and δ 1.70 were coupled to the Hs at δ 1.18 and δ 1.52; the H at δ 1.50 was coupled to the methylene Hs at δ 1.34 and δ 1.20 which were in turn coupled to the H at δ 1.63; the carbinyl Hs at δ 4.21 and δ 3.45 were coupled to each other.

Correlation of the partial structures deduced from the COSY spectrum and the data from the ^1H, ^{13}C, DEPT NMR, FT-IR and MS, as well as comparison with the structures of compounds previously isolated from *L. camara* resulted in structure **1**.

The ^1H NMR spectrum of **2** showed resonances for olefinic Hs at δ 5.39 and δ 5.60; carbinyl Hs of an ether or alcohol at δ 3.90 and δ 4.21; a carbinyl H of an ester at δ 4.95; allylic methyl groups at δ 2.15 and δ 1.88; and six methyl groups at δ 1.18; δ 1.08, δ 1.04, δ 0.92 ($2CH_3$), and δ 0.79 (Table 2). Comparison of the ^1H NMR data of **1** and **2** indicated that the differences between the two compounds are the esters attached to the triterpenes. The ester of **1** is an acetate (δ 2.0), while that of **2** is a dimethylacrylate (δ 1.88, δ 2.15, δ 5.6).

To support the structure of **2**, the ^{13}C NMR spectra of **1** and **2** were compared (Table 2). The spectrum indicated thirty-five carbons in **2** with the following changes in functionalities: an additional olefin (157.0 and 116.0 ppm), a deshielded carbonyl carbon (165.4 ppm) due to conjugation, and an additional methyl group.

The structure of **3** was deduced by subtracting the resonances of **2** from the ^{13}H NMR spectrum of a mixture of **2** and **3**. The olefin H at δ 6.00 (m) and the methyl Hs at δ 1.04 (d) indicated that the ester substituent of **3** is an angelate.

Compounds **2** and **3** have been reported as constituents of *L. camara* with pink flowers, but they have not been purified [9]. This is the first time that **2** was obtained pure and characterized.

The structure of **4** deduced by comparison of its ^1H NMR spectrum with the spectra of **1-3** (Table 1). The resonances for the ester substituents of **1-3** were not found in **4**. In addition, the resonance for the carbinyl H (δ 4.95) was not found in **4**. Thus, **4**, is the unsubstituted triterpene, lantanolic acid [9].

The structure of 5 was elucidated by comparison of its ^1H NMR spectral data with that of **4** (Table 1). Compounds **1** and **4** have similar spectral data, except for the presence of six methyl singlets in **4**, while **5** has four methyl singlets and two methyl doublets.

Table 3. Antimicrobial Index

Bacterium	*1*	*Chloramphenicol*	*Tetracycline*	*Acetone*
E. coli	0.2, 0		1.5	
S. aureus	0.7, 1.2	1.5, 1.7		
P. aeruginosa	0.1, 0.2		0.6, 0.5	0.1, 0.2
S. typhi	0.4, 1.0		0.8, 0.8	0.1, 0.2
Fungus		*Clotrimazole*		
C. albicans	0.2, 0.2	4.0, 3.0		0.2, 0.2
T. mentagrophytes	2.3, 2.3	5.0, 4.0		2.0, 2.1

L. camara is known to have antimicrobial properties. Thus, **1** was tested for its antimicrobial potential by the use of the well method. Results of the study are presented in Table 3. Among the six microorganisms tested, **1** was found to be active against *S. aureus* and *S. typhi* with an average antimicrobial index of 0.95 and 0.55, respectively at a concentration of 30 μg/mL.

The antimutagenicity potential of **1** was also tested by the use of the micronucleus test. Results of the study indicated that **1**, at a concentration of 6.75 mg/kg mouse, reduced the number of micronucleated polychromatic erythrocytes induced by Mitomycin C by 76.7%. Statistical analysis using the T-test showed that there is a significant decrease in MPCE at $\alpha = 0.01$. Therefore, **1** possesses a high antimutagenic activity.

CONCLUSION

Our investigation of the chloroform extract of the leaves of pink-flowered *L. camara* thus afforded a new triterpene **(1)**, **2**, a mixture of **2** and **3**, **4**, and **5**. Results of the antimicrobial test on **1** indicated that it is active against *S. aureus* and *S. typhi*, while results of the micronucleus test indicated that it has a high antimutagenic activity.

ACKNOWLEDGMENT

A research grant of the Department of Science and Technology is gratefully acknowledged. The antimicrobial test was conducted by the National Science Research Institute at UP Diliman.

REFERENCES

1. W.D.Bonner. Plant Biochemistry. 1950. Academic Press, Inc., New York. p. 384.
2. L. Co. Common Medicinal Plants of the Cordillera Region. 1989. p. 63.
3. P.G. Louw Onderstepoort. *J. Vet. Sci.* 1943. 18:197.
4. D. Barton, R. de Mayo, and J. Orr. *J. Chem. Soc.* 1956. 4160.
5. A. Barua, P. Sanyal, B. Das, and K. Charbabarti. *J. Indian Chem. Soc.* 1969. 46(1): 100-101.
6. J.M. Herbert and M. Maffrand. *J. Nat. Prod.* 1991. 54(6): 1595-1560.
7. O. Sharma, *J. Sci. and Ind. Res.* 1969. 48: 471.
8. N. Hart and A. Suares. *Australian J. Chem.* 1976. 29: 655-671.

THE FEASIBILITY OF USING IPIL-IPIL GUM AS AN ALTERNATIVE TO GUAR GUM

MA. VILMA D. FAUSTORILLA[1], BENIGNO D. PECZON[1], and IRENE M. VILLASEÑOR[2]

[1] *United Laboratories, United Street*
1550 Mandaluyong City

[2] *Institute of Chemistry, College of Science*
University of the Philippines Diliman
1101 Quezon City

ABSTRACT

Currently, most of the excipients used in the pharmaceutical industry are imported. In 1993, the Philippines imported a total of 278,262 kg of guar gum. The estimated gum consumption of the pharmaceutical industry is 156,74 kg/year.

A locally grown plant that can be tapped for gum production is *Leucaena leucocephala* (Lam.) de Wit, locally known as ipil-ipil. The crude gum from the seeds of the plant was purified by fractional precipitation with ethanol followed by ion exchange chromatography using a DEAE-cellulose column. Physicochemical and chemical studies showed that the protein-free gum exhibited properties similar to that of galactomannan from guar gum. A hardness test performed on tablets formulated with the purified gum showed that the gum is an effective binder.

A summary of a pre-feasibility study on the commercialization of ipil-ipil seed gum is discussed.

SURFACE SENSITIVE ANALYSIS OF THIN OXIDE FILMS ON SEMICONDUCTORS

TERENCIO D. LACUESTA[1], TERRENCE JACH[2], and STEPHEN M. THURGATE[3]

[1]*Institute of Mathematical Sciences and Physics*
University of the Philippines Los Baños
College, 4031 Laguna

[2]*National Institute of Standards and Technology*
US Department of Commerce
Gaithersburg, Maryland 20899
U.S.A.

[3]*School of Mathematical and Physical Sciences*
Murdoch University
Murdoch, Western Australia 6150

ABSTRACT

Oxide layers on semiconductor-based electronic devices play an important role in the performance of the device. Thicknesses of about 5 nm are projected for future designs. Common commercial cleaning and etching preparations of the semiconductor materials produce oxide layers with a thickness in this range. The oxidized surface of indium phosphide (InP) was studied. The techniques of Auger Electron Spectroscopy (AES) and Grazing Incidence X-ray Photoelectron Spectroscopy (GIXPS) were employed. These techniques provide a truly surface sensitive analysis of the material. The native oxide on InP was measured to have a thickness of about 2.0 nm. The chemical composition of the layer was also obtained.

INTRODUCTION

Modern electronic equipment and instrumentation make use of an array of a large number of semiconductor devices. Many of these devices are in fact integrated into a smaller electronic component called integrated circuits (ICs) or "chips".

ture shown in Figure 1. The metal serves as the gate to which a voltage is applied: Electrons move from the source to the drain through some channels in the semiconductor material.

A similar structure used extensively as an electronic device is the metal-oxide-semiconductor (MOS). Instead of using an insulator to separate the metal and the semiconductor, an oxide of the semiconductor is grown. This is typical in silicon based field effect transistors (FET). The native oxide SiO_2 is produced during the preparation of the silicon wafers. Metal contacts are connected onto the oxide.

Another device structure also extensively used is the metal semiconductor junction found in diodes. The metal gate is bonded directly onto the semiconductor. However, under normal atmospheric conditions, oxide growth on both the semiconductor and the metal is not totally eliminated. A negligible amount of the oxide may not hinder usual functions of the device but future degradation and instability in performance is anticipated.

The quest for faster and improved devices led to the search for other semiconductors. Indium phosphide (InP) and gallium arsenide (GaAs) are now used in view of their faster electron mobilities and more efficient photon energy conversion compared to silicon. However, the chemical stability of the phosphorus oxides over the arsenic oxides make InP a better material for MIS/MOS devices while GaAs is preferred for metal semiconductor devices.

The current trend toward smaller device areas and thinner insulating layers is evident in the miniaturization and compactness of new electronic equipment. Oxide layers of the future are expected to have a thickness of about 5 nm (1 nm = 10^{-9} m) compared to present day devices with oxide thicknesses of about 1 μm (10^{-6} m). It is therefore necessary that a method of sampling thin layers of the oxide and the semiconductor and metallic surfaces be used to determine the chemical species present on the interface. A knowledge of the composition of the interface can give us an insight on the performance of a fabricated device.

There have been diverse tools and applications of surface characterization since the 1970s.[2,3] The volume of papers published on studies of surfaces has grown significantly since then that the field is now widely accepted as surface science.

All surface analyses techniques use a probe to excite the materials and information about their surfaces is obtained by detecting quantities emitted from the surface. Common excitation probes make use of photons, electrons, ions, neutral particles, phonons, or electromagnetic fields. The detected quantities may be particles (photons, electrons, ions, neutral atoms, or phonons) or fields (electric or magnetic).

In this study, two of the most common techniques were employed to study the oxide layer on indium phosphide, namely, Auger Electron Spectroscopy (AES) and Grazing Incidence X-ray Photoemission Spectroscopy (GIXPS). These two techniques are the most advantageous over other methods.[3]

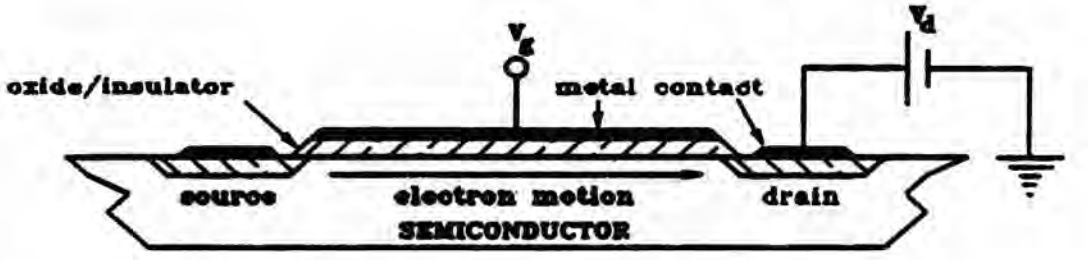

Figure 1. Schematic diagram of a MOS/MIS structure.

EXPERIMENTAL DESCRIPTION

Surface analyses techniques are carried out in an ultra high vacuum (UHV) environment typically with ultimate pressures of 10^{-9} to 10^{-10} torr. This ensures that the excitation probe will reach the sample without undergoing collisions or interaction with the ambient gas. Likewise, the sample surface will not be subjected to prolonged contamination from the ambient.

The specimen is then bombarded by x-rays for X-ray Photoemission Spectroscopy (XPS) and electrons or x-rays for AES. Electrons are emitted from the sample and are detected and analyzed.

For AES, the specimen is usually bombarded with electrons having energies between 2 and 15 keV. Core level ionizations of the specimen atoms decay by either the emission of characteristic x-ray or the emission of Auger electrons. The Auger process is a two-electron decay process wherein an electron from a higher level in the atom fills the initial core level vacancy and another electron from the same or another level is emitted. The kinetic energy of the emitted electron called the Auger electron is related to the binding energy of the electron in the level which was initially ionized and of the two electrons which participated in the process. Figure 2 shows a schematic diagram of the process of Auger electron emission. The kinetic energies of electrons emitted from the specimen are measured with an electron analyzer which measures the Auger electron distribution. Peaks in this distribution correspond to Auger electrons that leave the specimen without inelastic scattering and with characteristic energies which are used to identify specific atoms.

For XPS, characteristic x-rays from the anode (often Mg or Al) of a relatively simple x-ray tube excite photoelectrons from core levels (when energetically possible) of the specimen. The photoelectrons that emerge from the specimen in a

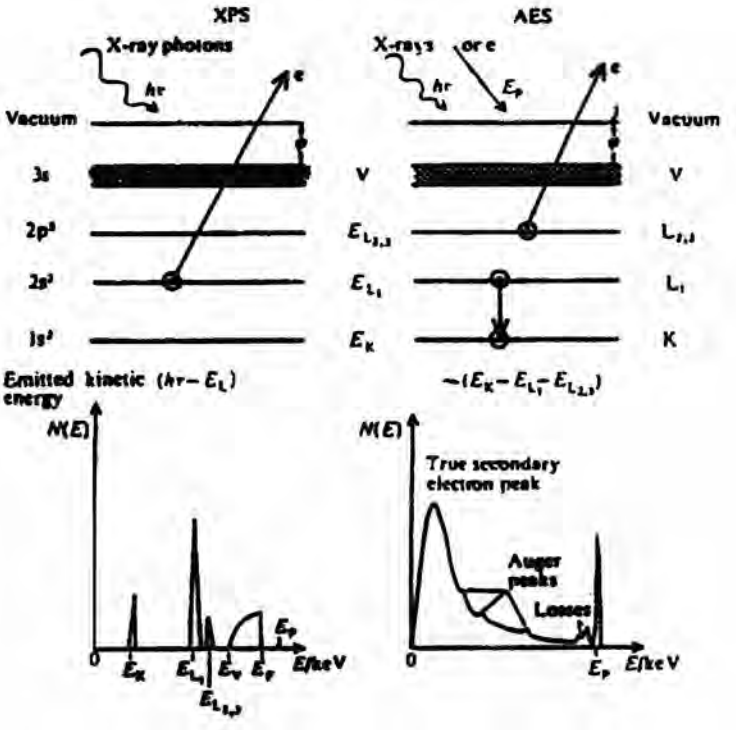

Figure 2. Schematic diagram of X-ray photoemission and Auger electron processes. Energy levels are that of an ideal free one-electron metal (not drawn to scale). The quantities on the left are the electronic configuration. At the right are the labels for orbitals used in X-ray spectroscopy. E_K is the binding energy measured from the vacuum level. The graphs at the bottom indicate the number $N(E)$ of electrons with kinetic energies between E and $E + dE$ measured in the energy distribution. The horizontal scale corresponds to what is obtained in common practical cases.

particular direction enter an electron energy analyzer (similar as in AES) which measures the photoelectron energy distribution. Peaks in this photoelectron energy distribution correspond to photoelectrons from core levels that emerge without inelastic scattering in the specimen. The kinetic energies of the photoelectrons contributing to these peaks are related to core level binding energies which can be used for elemental identification. The shapes and energies of these peaks also provide information on the chemical states of the sample since the binding energies depend on the chemical environment.

Auger peaks are also observed in XPS where the core level vacancies are created by x-rays. These however cause interference and complicate the spectra. Nonetheless, they provide reference energies and Auger related information. The photoelectron peaks are narrower and simpler than the Auger peaks. The valence spectra are generally very weak in XPS but are dominant in AES. The energies of peaks in both sets of spectra are in the same range. This means that the depth to

which the surface is analyzed is quite similar for both techniques since it is the energy of the ejected electrons that determine the analyzed depth rather than the energy of the excitation beam. The surface sensitivity of both techniques is due to the very short inelastic mean free paths of photoelectrons and Auger electrons (0.2-2.0 nm) in most solids in the energy range of 30-2000 eV normally used. Photoelectrons and Auger electrons emitted deeper in the specimen have a much greater chance of being inelastically scattered than those emitted near the surface. Thus, only the electrons emitted from near the surface will be detected.

Table 1 summarizes the major advantages and limitations of AES and XPS for surface analyses. Both techniques are complementary and may be carried out with the same analyzer in situ. X-ray excitation is used for the reason that it causes the least damage on the sample being analyzed. The use of electron beams for core level ionization are preferred because the electron sources are normally "brighter" than x-ray sources. Electron beams of small diameter may be easily produced to provide better lateral imaging. Since the x-rays are more energetic than the electron beams often used, x-rays have deeper penetration (up to 1μm) into the sample than the electron beams. This makes AES a more surface sensitive technique.

Figure 3 shows an experimental apparatus for the GIXPS measurements. The electron energy analyzer is the cylindrical mirror analyzer (CMA) with a built in electron gun in the axis of the CMA for AES. The electron beam is at normal incidence to the sample. However, AES measurements in this study were performed in another UHV chamber. A laboratory Mg K_α x-ray tube was used. It is usually at large angles (relative to the sample plane) of x-ray incidence for the usual XPS measurement. For GIXPS measurements, the x-ray tube was mounted on the radial track with angular adjustment to focus the x-ray beam at a low angle of incidence (grazing incidence) relative to the sample surface plane. This gave an angular resolution of 0.1°.

AES was performed in a similar chamber but using a three grid LEED optics as energy analyzer. Beam energies of 2.5 keV and a current 4 μA were used. An ion gun is also available for ion milling or bombardment of the surface to remove contamination. The ion milling procedure is done for depth profile studies of the surface. The ion gun may be introduced into any port of the chamber and the sample holder is just rotated until the sample is in the direct line of the ion beam for the ion milling procedure.

Depth profile studies of the sample surface were carried out by monitoring the composition of the surface using AES. The surface was ion bombarded with a geometrically increasing ion dose. The elemental intensities as a function of ion dose was measured and the thickness of the oxide layer was deduced.

Elemental identification using AES is routine but compositional analysis is mainly qualitative. A quantitative study of the chemical states on the surfaces is often tedious since the quantitative analyses involve considerations of the elemental sensitivity factors and inelastic mean free paths which are available from reference standards.

Table 1. Major advantages and limitations of AES and XPS.

	AES	XPS
Advantages	Sensitive to 2-20 monolayers Can detect *ca.* 10^{-3} atomic fraction Has a sensitivity range within a factor of 20	
	Has superb lateral resolution Can acquire data rapidly Gives chemical information for some elements	Has minimal sample charging Least destructive of all techniques Useful for chemical states of the same element in different compounds
Limitations	May alter surface composition Severe charging problems for nonconducting elements	Has moderate lateral resolution Slower depth profiling than other methods

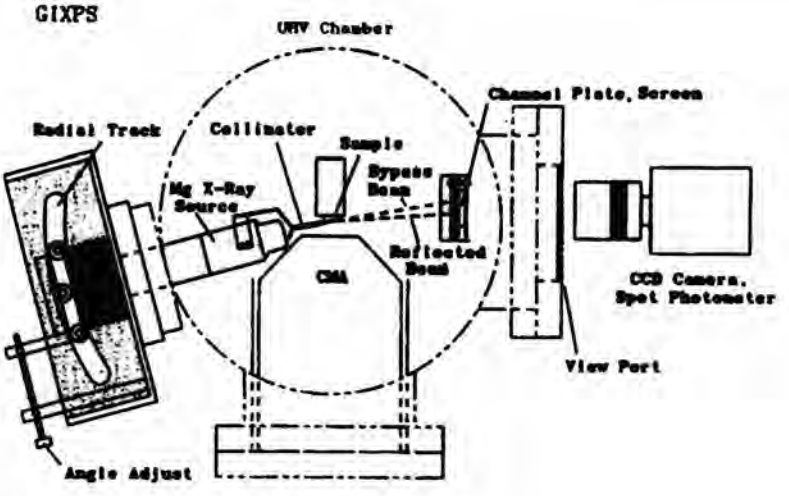

Figure 3. Experimental apparatus

Chemical state information of a surface is best obtained using XPS. However, as the incidence angle of the x-rays is increased, the x-ray penetration depth increases and the photoelectron yields contain a larger contribution from deeper layers within the sample. For XPS x-rays, the refractive indices of materials are slightly less than unity so that a beam of x-ray incident on a flat surface at small incidence angles ($< 3^{\circ}$) undergoes total external reflection. GIXPS takes advantage of this property. Hence there is an enhancement of photoelectron yields from the surface region.

Figure 4 shows a plate image of the reflected x-ray beam from a GaAs wafer with a standard commercial polish and the bypass beam when the sample holder

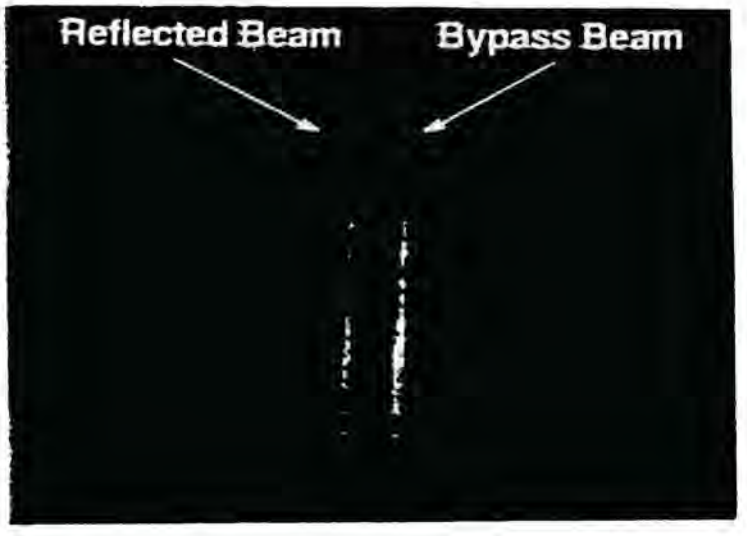

Figure 4. Channel plate image of bypass x-ray beam and reflected beam from a GaAs wafer with a standard commercial polish.

was slightly rotated so that the x-ray did not hit the sample. It may be seen that the intensities of the beams are very similar indicating the total external reflection of x-rays.

Chemical information from XPS is obtained from the peak intensities of photoelectrons from specific elements. Electrons in atoms have definite binding energies so that with a constant x-ray source energy, the photoelectrons have definite kinetic energies. Thus for pure elemental samples the photoelectron distribution is very narrow, occurring at definite energies. Standard peak positions are available for many elements. The peak distribution assumes a normal Gaussian Lorentzian distribution.

If the elements are present in different compounds, the electron binding energies are shifted reflecting the chemical environment. The photoelectron peak distributions are shifted. Because the photoelectron yields come from the pure elements and the compound atoms, the peaks assume broad and skewed line shapes. Curve fitting is done by assuming the superposition of several normal Gaussian distributions under the observed broad peaks. Each fitted Gausian distribution corresponds to a definite chemical state with known binding energy. Thus the chemical species on the surface may be determined as well as their concentrations based on the relative areas (or intensities) under the peak distribution.

Several InP (100) wafers were prepared using different etches. Chemical polishing was performed using 0.1-2.0% Br in methanol solutions followed by etching in either acidic or basic solutions. The acidic etchants used were mainly HF or HNO_3 while the basic etchant was 1M NaOH. All reagents used were analytical grade in their normal commercial concentrations. Etching time was 2.0 min for all

etches and the samples were dried in a stream of dry nitrogen and immediately inserted into the UHV chamber.

RESULTS AND DATA ANALYSIS

Figure 5 shows AES derivative spectra from the different surface preparations. The derivative spectra were analyzed because the direct spectra were very broad. The Ar^+ ion bombarded surface may be considered to be clean or contamination–free since the bombardment procedure would have sputtered off the contaminants. The main features of the clean surface are the P and In valence peaks at 120 and 430 eV respectively. Indium satellite peaks in the lower energy side of In are due to Auger electrons coming from deeper levels of the atom. Shorter spectra with small energy intervals for the different valence Auger electrons of P, C, In, and O were also obtained.

The contaminants on the etched surface are mainly carbon and oxygen. It can be seen that the NaOH etched surface contains large oxygen contamination and minimal carbon coverage while the HF etched surface has larger carbon coverage and less oxygen contamination.

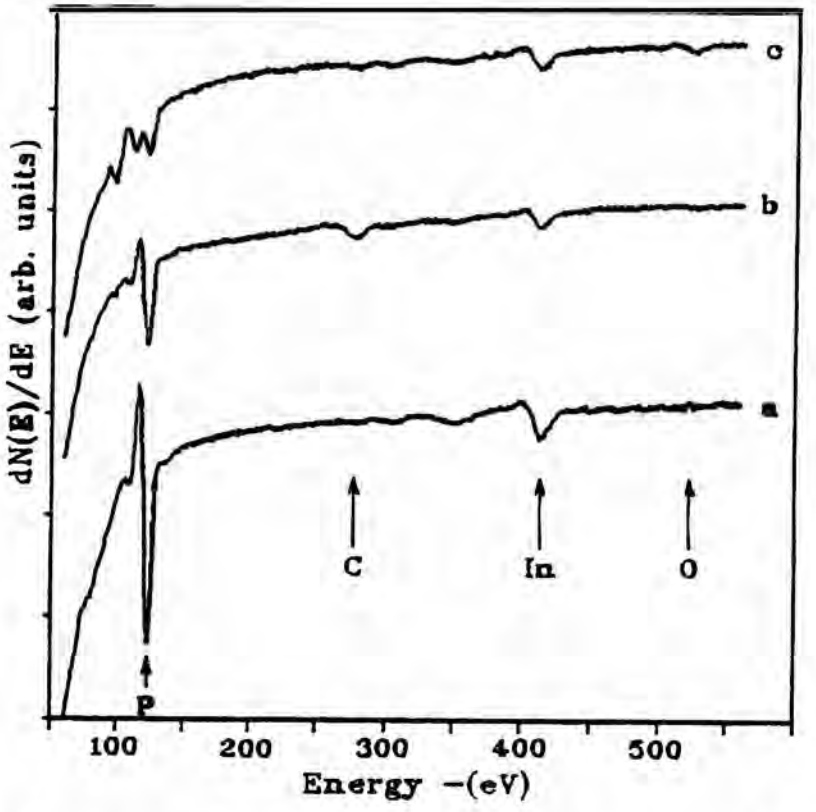

Figure 5. Auger spectra from InP for various surface treatments: *(a)* Ar^+ ion bombarded; *(b)* HF etched; and *(c)* NaOH etched.

Depth profile studies of the etched surfaces were performed with cumulative bombarding times of 0.5, 1, 2, 4, 8, 16, 32, and 60 min. Intensity measurements on the AES spectra after each bombardment procedure were obtained and shown in Figure 6. Based on the increase in the phosphorus intensity and using an escape depth of 0.966 nm for phosphorus Auger electrons in InP[4], the approximate oxide thicknesses for the different surface treatments were deduced and shown in Table 2.

The oxygen coverage on the NaOH etched surface is quite different from that of the HF etched surface. Careful inspection of the oxygen peaks in both surfaces shows that the oxygen peak position of the NaOH etched spectrum is different from the HF etched spectrum. Moreover, the satellite peaks on the lower energy side of the phosphorus peak of the NaOH etched spectrum are indicative of interatomic transitions[5] during the Auger decay. The interatomic transition arises when an electron from the oxygen fills the initial vacancy created in the phosphorus. This

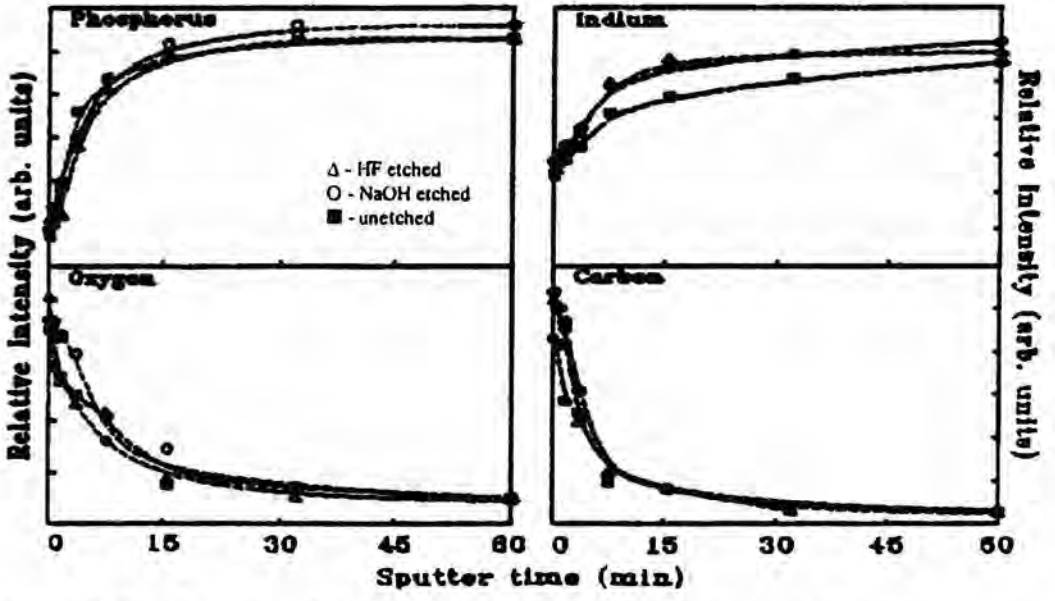

Figure 6. Depth profile of HF, NaOH, and uneteched InP samples.

Table 2. Native oxide thickness on InP obtained by different surface treatments.

Surface Treatment	Oxide Thickness
HF etched*	1.5 ± 0.2 nm
NaOH etched*	2.3 ± 0.4 nm
HNO3 etched+	1.8 ± 0.1 nm

*AES +GIXPS

is possible because of the proximity of oxygen to phosphorus in compounds of phosphorus oxides (P_xO_y). For the HF etched surface which has the minimum oxygen coverage, careful analysis of the oxygen peaks in the depth profile spectra gave an approximate oxygen coverage of about 14%. Oxygen levels in the NaOH etched surface are obviously larger.

Spectra from the GIXPS on the HNO_3 etched sample were taken at six angles of incidence for each of the following lines: in $3d_{5/2}$, O 1s, P 2p, and C 1s. The photoemission peaks were fitted for the compounds reported by Hollinger et al.[6] to be stable compounds on the surface of InP. These are In_2O_3, $InPO_4$, $In(OH)_3$, H_2O, and C. However, binding energies assigned by Thurgate and Erickson[7] which are slightly modified from the values of Hollinger et al.[6] were used. Figure 7 shows a sample spectrum of the In $3d_{5/2}$ line taken at an incidence angle of 55 mrad. The spectrum shows the photoemission peak and the fits of the different chemically shifted constituents.

Simultaneously fitting procedures were also performed on the other spectral lines. By analyzing the fits for the elements that are correlated in a single compound, several observations were made:

1. The surface was covered in a single thin layer. The oxide had not separated into distinct component layers of $InPO_4$ and In_2O_3 as reported for thicker oxides[8].

2. The overlayer had a thickness of 1.8 nm (assuming a mean free path of 2.0 nm) in the overlayer for an electron with a kinetic energy of 1250 eV), a composition of 83% C, 13% O, 4% In, and a density equal to the density of the substrate.

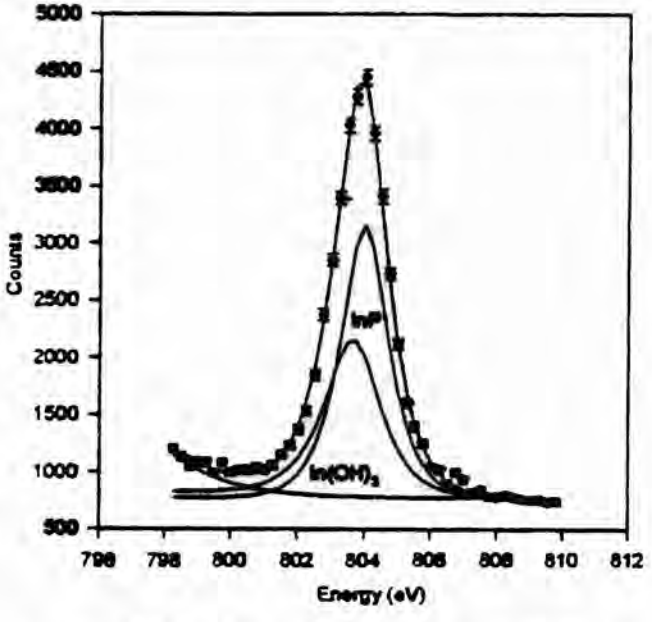

Figure 7. Decomposition of the Indium $3d_{5/2}$ line wih an incidence angle of 55 mrad. The In component of $InPO_4$ is so small that it has not been included.

CONCLUSIONS

From this study, it was observed that acidic solutions produce thinner oxides than basic solutions. On the other hand there is larger carbon contamination in the acidic etch but larger oxygen incorporation in a basic etch. The kinetics of the dissolution of elements on the surface may be considered. The dissolution of InP to phosphoric acids is thermodynamically favorable[9] in acidic media and is discharged into the solution until it becomes saturated with the aqueous phosphates. This leaves the surface indium rich in the form of hydrated indium oxides[10] which in turn readily absorb CO_2 from the atmosphere. This explains the high carbon coverage in the acidic etches.

In the basic solutions, phosphates appear in the form of HPO^{2-} and PO_4^{3-} which in the presence of the hydroxyl ions (OH^-), reprecipitate[9] onto the surface. This accounts for the large quantities of phosphate species on the NaOH eteched surface. The phosphate surface covers the indium oxides preventing them from absorbing large amounts of carbon dioxide.

Finally, since the GIXPS technique provided a surface sensitive chemical analysis of the sample, the observed phosphorus peak from the AES study of the HF etched surface may be considered to emanate from deeper levels. This is not surprising since the electron beam used in AES is at normal incidence to the surface and therefore has greater penetration depths.

We conclude that acidic etchants produce thin oxide overlayers on InP. This is in agreement with the results on InP obtained by Kirk and Jones[11]. It is viable to use acidic etchants for InP water preparation to obtain thin oxide layers. However, this layer consists of a heterogeneous mixture of $In(OH)_3$, and In_2O_3, C, and very little $InPO_4$. This surface looked similar to the surface prepared and analyzed using angle resolved XPS by Zemek et al.[12] The presence of indium phosphate as found by Hollinger et al.[6] may be located at the InP substrate but beneath the indium hydroxide.

Finally, GIXPS and AES are complementary techniques that provide very good compositional and chemical analyses of very thin oxide layers.

ACKNOWLEDGMENTS

T.D. Lacuesta would like to thank the Engineering and Science Education Project (ESEP) of the Department of Science and Technology and the Australian International Development Assistance Bureau (AIDAB) for the fellowship grants.

LITERATURE CITED

[1]C.J. Powell, *Crit. Rev. Surf. Chem.* **2**(1,2):17 (1993).

[2]C.J.Powell, *Appl. Surf. Sci.* **1**:143 (1978).

[3]J.E. Fulghum, G.E. McGuire, I.H. Musselman, R.J. Nemanich, J.M. White, D.R. Chopra, and A.R. Chourasia, *Anal. Chem.* **61**:243R (1989).

[4]M.P. Seah and W.A. Dench, *Surf. Int. Anal.* **1**(1):2 (1979).
[5]R.H. Williams and I.T. McGovern, *Surf. Sci.* **51**:14 (1975).
[6]G. Hollinger, E. Bergignat, J. Joseph, and Y. Robach, *J. Vac. Sci. Technol.* **A3**:2080 (1985).
[7]S.M. Thurgate and N.E. Erickson, *J. Vac. Sci. Technol.* **A8**:372 (1990).
[8]C.W. Wilmsen and R.W. Kee, *J. Vac. Sci. Technol.* **14**:953 (1977).
[9]A.P. Tomilov and N.E. Chomutov, Encyclopedia of Electrochemistry of the Elements, A.J. Bard, ed. Vol. VI:1, New York: Marcel Dekker, Inc. (1976).
[10]V.V. Losev and A.I. Molodov, *Encyclopedia of Electrochemistry of the Elements*, A.J. Bard, ed., Vol. VI:1, New York: Marcel Dekker, Inc. (1976).
[11]D.L. Kirk and C. Jones, *J. Appl. Phys.* **12**:651 (1979).
[12]J. Zemek, O.A. Baschenko, and M.A. Tyzkov, *Thin Solid Films* **224**:141 (1993).

RUNGE-KUTTA METHODS AND UNIFORMLY REGULAR MATRICES

EMMANUEL M. LAGARE[1,3] and BIBIANO O. PUYOS[2]
[1]*Department of Mathematics*
MSU-Iligan Institute of Technology
Tibanga, 9200 Iligan City

[2]*Mathematics Department*
MSU-Marawi City, 9700 Marawi City

ABSTRACT

Uniformly regular matrices can be used for approximating the integral of the a function on a given interval. Considering that Runge-Kutta methods use weights to arrive at an approximation to the solution of a differential equation, whenever it exists, applying uniformly regular matrices to Runge-Kutta methods is a natural step to take. The class of uniformly regular matrices is large so we ask what properties do we need to have to be able to use such matrices. This paper gives sufficient conditions for the application of uniformly regular matrices to Runge-Kutta methods of order 2 and order 3 as well as some examples.

Unformly regular matrices were used by Lee [5] and Lagare [2, 3, and 4] to find the approximation of the integration of a given function f on the interval $[a, b]$. Knowing the intimate connection between integrals and solutions to differential equations, it is natural to ask if uniformly regular matrices can be used to approximate the solution to a differential equation.

One way of solving a differential equation is to use integration methods and this is essentially covered in the above works. Another method we can apply uniformly regular matrices to is Runge-Kutta methods. This is because Runge-Kutta methods use weight in the algorithm to approximate the solution to the given differential equation. In this paper, we give sufficient conditions

[3]The author thanks Director Wilfredo A. Dimamay of the MSU-IIT Computer Center for the use of the computing facilities of the Center in this work.

on uniformly regular matrices so they can be used for Runge-Kutta methods of orders 2 and 3. We also give an example showing several computations approximating the solution to a differential equation.

Runge-Kutta methods are self-starting methods and are easy to program on a computer but it is at a disadvantage when error-estimation and speed are considered. When the derivative is simple, Runge-Kutta methods can be competitive in terms of speed. Moreover, by using additional evaluations of the function, a good error estimate can be obtained. The objective of this paper is to find a way of cheaply finding the weights for the method that will contribute to its further use.

Given a differential equation

$$\frac{dy}{dx} = f(x, y) \quad y(x_o) = y_o,$$

we assume it to posses a solution, $y(x)$, which is unique, continuous, and differentiable on $[x_o, b]$. Then Runge-Kutta methods can be generally written (c.f. [1] and [6]) as

$$y_{n+1} = y_n + \sum_{i=1}^{m} \omega_i k_i \tag{1}$$

where the ω_i 's are constants and

$$k_i = hf\left(x_n + \alpha_i h, y_n + \sum_{j=1}^{i-1} \beta_{ij} k_j\right)$$

with h denoting the difference and

$$x_{k+1} - x_k, \; x_0 < x_1 < \ldots < x_l = b.$$

The ω_i *'s,* α_i*'s and* β_{ij}*'s* are referred to as the parameters of the method.

The Taylor's Series expansion of y_{n+1} in (1) can be written as

$$y_{n+1} = y_n + \sum_{t=1}^{\infty} h^t y_n^{(t)} / t!$$

where

$$y_n^{(t)} = \frac{d^{t-1}}{dx^{t-1}} f(x_n, y_n) = \left(\frac{\partial}{\partial x} + \frac{dy}{dx}\frac{\partial}{\partial y}\right)^{t-1} f(x_n, y_n)$$

$$= \left(\frac{\partial}{\partial x} + f(x, y)\frac{\partial}{\partial y}\right)^{t-1} f(x_n, y_n).$$

On the other hand, the expansion for

$$f\left(x_n + \alpha_i h, y_n + \sum_{j=1}^{i-1} \beta_{ij} k_j\right)$$

is given by

$$f\left(x_n + \alpha_i h, y_n + \sum_{j=1}^{i-1} \beta_{ij} k_j\right) =$$

$$\sum_{t=1}^{\infty}\left[hD_i + \sum_{j=2}^{i-1} \beta_{ij}(k_j - hf(x_n, y_n))\frac{\partial}{\partial x}\right]^t f(x_n, y_n)/t!$$

where

$$D_i = \alpha_i \frac{\partial}{\partial x} + \left(\sum_{j=1}^{i-1} \beta_{ij}\right) f(x_n, y_n)\frac{\partial}{\partial y}.$$

Equating the left- and right-hand sides of (1) and matching the corresponding powers of h, we obtain a system of equations that will allow us to solve for the values of the ω_i's, α_i's, and β_{ij}'s. The order of the method will be the highest power m of h which we decide to retain in our expansion.

For Runge-Kutta methods of orders 2 and 3, we obtain the following systems:

For $m = 2$:

$$\begin{aligned} &\omega_1 + \omega_2 = 1 \\ &\alpha_1\omega_2 = 1/2 \\ &\alpha_2 = \beta_{21} \end{aligned} \tag{2}$$

Form $m = 3$:

$$\begin{aligned} &\omega_1 + \omega_2 + \omega_3 = 1 \\ &\alpha_2\omega_2 + \alpha_3\omega_3 = 1/2 \\ &\alpha_2^2\omega_2 + \alpha_3^2\omega_3 = 1/3 \\ &\alpha_2\beta_{32}\omega_3 = 1/6 \\ &\alpha_2 = \beta_{21} \\ &\alpha_2 = \beta_{31} + \beta_{32}. \end{aligned} \tag{3}$$

Each of the above systems have more variables than there are equations, so we can choose the free parameters to suit desired properties we want in the method.

Now let $A = (a_{n,k})$ be a row-finite matrix, that is, $a_{n,m(n)} \neq 0$ for all n, and $a_{n,k} = 0$ when $k > m(n)$. A row-finite matrix A is said to be uniformly regular if it satisfies the following three conditions:

(i) $\lim_{n \to \infty} a_{n,k} = 0$ uniformly in k,

(ii) $\lim_{n \to \infty} \sum_{k=1}^{m(n)} a_{n,k} = 1$, and

(iii) $\sup_{n \geq 1} \sum_{k=1}^{m(n)} |a_{n,k}| < +\infty$.

Theorem: Let A be a uniformly regular matrix whose ith row satisfies the following:

a) $a_{ij_1} > 0$, $a_{ij_2} > 0$, $a_{ij_3} > 0$ and $a_{ij_k} = 0$ for $k \neq 1, 2, 3$;

b) $a_{ij_3} \neq 3/4$;

c) $a_{ij_2} + a_{ij_3} \geq 3/4$; and

d) $a_{ij_1} + a_{ij_2} + a_{ij_3} = 1$.

Then the ith row can be used for the values of the parameters ω_1, ω_2, and ω_3 of a Runge-Kutta method of order 3, with $\omega_1 = a_{ij_1}$, $\omega_2 = a_{ij_2}$, and $\omega_3 = a_{ij_3}$. The values of the other parameters can be found using (3) and the values of ω_2 and ω_3.

For an order 2 method, the sufficient conditions are: $a_{ij_1} + a_{ij_2} = 1$ and $a_{ij_1} \neq 0$ with $a_{ij_k} = 0$ for $k \neq 1, 2$.

Proof: Solve the systems (2) and (3) and use the results with the properties of uniformly regular matrices.

Example: Given the initial value problem

$$y'(x) = y(x),\ y(0) = 1,\ b = 2.$$

The solution to the differential equation at the point $x = 2$ using Runge-Kutta methods of orders 2 and 3 are as follows:

R-K Order 2, $h = 1.0$

	Parameters			
y_n	$\omega_1 = 0$; $\omega_2 = 1$; $\alpha_2 = 0.5$; $\beta_{21} = 0.5$	$\omega_1 = 0.25$; $\omega_2 = 0.75$; $\alpha_2 = 0.66666666666667$; $\beta_{21} = 0.66666666666667$	$\omega_1 = 0.5$; $\omega_2 = 0.5$; $\alpha_2 = 1$; $\beta_{21} = 1$	$\omega_1 = 0.3$; $\omega_2 = 0.7$; $\alpha_2 = 0.7142875$; $\beta_{21} = 0.7142875$
y_1	2.50000000000000	2.50000000000000	2.50000000000000	2.50000125000000
y_2	6.25000000000000	6.25000000000000	6.25000000000000	6.25000625000156

R-K Order 2, $h = 0.5$

	Parameters			
y_n	$\omega_1 = 0$; $\omega_2 = 1$; $\alpha_2 = 0.5$; $\beta_{21} = 0.5$	$\omega_1 = 0.25$; $\omega_2 = 0.75$; $\alpha_2 = 0.66666666666667$; $\beta_{21} = 0.66666666666667$	$\omega_1 = 0.5$; $\omega_2 = 0.5$; $\alpha_2 = 1$; $\beta_{21} = 1$	$\omega_1 = 0.3$; $\omega_2 = 0.7$; $\alpha_2 = 0.7142875$; $\beta_{21} = 0.7142875$
y_1	1.62500000000000	1.62500000000000	1.62500000000000	1.62500031250000
y_2	2.64062500000000	2.64062500000000	2.64062500000000	2.64062601562510
y_3	4.29101562500000	4.29101562500000	4.29101562500000	4.29101810058641
y_4	6.97290039062500	6.97290039062500	6.97290039062500	6.97290575439608

R-K Order 2, $h = 0.25$

	Parameters			
y_n	$\omega_1 = 0$; $\omega_2 = 1$; $\alpha_2 = 0.5$; $\beta_{21} = 0.5$	$\omega_1 = 0.25$; $\omega_2 = 0.75$; $\alpha_2 = 0.66666666666667$; $\beta_{21} = 0.66666666666667$	$\omega_1 = 0.5$; $\omega_2 = 0.5$ $\alpha_2 = 1$; $\beta_{21} = 1$	$\omega_1 = 0.3$; $\omega_2 = 0.7$; $\alpha_2 = 0.7142875$; $\beta_{21} = 0.7142875$
y_1	1.28125000000000	1.28125000000000	1.28125000000000	1.28125007812500
y_2	1.64160156250000	1.64160156250000	1.64160156250000	1.64160176269532
y_3	2.10330200195313	2.10330200195313	2.10330200195313	2.10330238670352

R-K Order 2, $h = 0.25$ *(continued)*

Parameters				
y_4	2.69485569000244	2.69485569000244	2.69485569000244	2.69485634728438
y_5	3.45278385281563	3.45278385281563	3.45278385281563	3.45278490549376
y_6	4.42387931142002	4.42387931142002	4.42387931142002	4.42388092991270
y_7	5.66809536775691	5.66809536775691	5.66809536775691	5.66809778706635
y_8	7.26224718993854	7.26224718993854	7.26224718993854	7.26225073249890

R-K Order 3, $h = 1.0$

Parameters				
y_n	ω_1=0.22222222222222 ω_2=0.33333333333333 ω_3=0.44444444444 α_2= 0.5; α_3= 0.75; β_{21} = 0.5; β_{31} = 0; β_{32} = 0.75;	ω_1 = 0.166666666666 7; ω_2 = 0.666666666666 7; ω_3 = 0.166666666666 7; α_2 = 0.5; α_3 = 1.0; β_{21} = 0.5; β_{31} = -1.0; β_{32} = 2.0;	ω_1 = 0.2; ω_2=0.4; ω_3=0.4 α_2 = 0.46362569390802; α_3 = 0.78637430609198; β_{21} = 0.46362569390802; β_{31} = -0.112339186584578; β_{32} = 0.89871349267654;	ω_1 = 0.2; ω_2=0.4; ω_3=0.4 α_2 = 0.7863743060919 8; α_3 = 0.46362569390802; β_{21} = 0.78637430609198; β_{31} = -0.066232241986861; β_{32} = 0.52985793589488;
y_1	2.666666666666 7	2.666666666666 6	2.666666666666 6	2.666666666666 7
y_2	7.111111111111 1	7.111111111111 1	7.111111111111 08	7.111111111111 1

R-K Order 3, $h = 0.5$

Parameters				
y_n	ω_1 = 0.22222222222222 ω_2 = 0.33333333333333 ω_3 = 0.44444444444 α_2 = 0.5; α_3 = 0.75; β_{21} = 0.5; β_{31} = 0; β_{32} = 0.75;	ω_1 = 0.166666666666 7; ω_2 = 0.666666666666 7; ω_3 = 0.166666666666 67; α_2 = 0.5; α_3 = 1.0; β_{21} = 0.5; β_{31} = -1.0; β_{32} = 2.0;	ω_1 = 0.2; ω_2=0.4; ω_3=0.4 α_2 = 0.46362569390802; α_3 = 0.78637430609198; β_{21} = 0.46362569390802; β_{31} = -0.112339186584578; β_{32} = 0.89871349267654;	ω_1 = 0.2; ω_2=0.4; ω_3=0.4 α_2 = 0.78637430609198; α_3 = 0.46362569390802; β_{21} = 0.78637430609198; β_{31} = -0.066232241986861; β_{32} = 0.52985793589488;

R-K Order 3, $h = 0.5$ *(continued)*

	Parameters			
y_1	1.64583333333333	1.64583333333333	1.64583333333333	1.64583333333333
y_2	2.70876736111111	2.70876736111111	2.70876736111111	2.70876736111111
y_3	4.45817961516204	4.45817961516204	4.45817961516203	4.45817961516204
y_4	7.33742061662085	7.33742061662085	7.33742061662083	7.33742061662085

R-K Order 3, $h = 0.25$

	Parameters			
y_n	ω_1 = 0.22222222222222 ω_2 = 0.33333333333333 ω_3 = 0.44444444444 α_2 = 0.5; α_3 = 0.75; β_{21} = 0.5; β_{31} = 0; β_{32} = 0.75;	ω_1 = 0.166666666666 7; ω_2 = 0.666666666666 7; ω_3 = 0.166666666666 7; α_2 = 0.5; α_3 = 1.0; β_{21} = 0.5; β_{31} = −1.0; β_{32} = 2.0	ω_1 = 0.2; ω_2 = 0.4; ω_3 = 0.4 α_2 = 0.46362569390802; α_3 = 0.78637430609198; β_{21} = 0.46362569390 ; β_{31} = -0.112339186584578; β_{32} = 0.89871349267654;	ω_1 = 0.2; ω_2 = 0.4; ω_3 = 0.4 α_2 = 0.78637430609198; α_3 = 0.46362569390 ; β_{21} = 0.78637430609198; β_{31} = -0.066232241986861; β_{32} = 0.52985793589488;
y_1	1.28385416666667	1.28385416666667	1.28385416666667	1.28385416666667
y_2	1.64828152126736	1.64828152126736	1.64828152126736	1.64828152126736
y_3	2.11615309891877	2.11615309891877	2.11615309891877	2.11615309891877
y_4	2.71683197335145	2.71683197335145	2.71683197335144	2.71683197335145
y_5	3.48801604912048	3.48801604912048	3.48801604912047	3.48801604912048
y_6	4.47810393806353	4.47810393806353	4.47810393806352	4.47810393806353
y_7	5.74923239964927	5.74923239964927	5.74923239964926	5.74923239964927
y_8	7.38117597142471	7.38117597142471	7.38117597142470	7.38117597142472

The results in the first two columns in each table are obtained using popularly recommended Runge-Kutta methods while the ones in the last two columns are Runge-Kutta methods using parameters selected based on the theorem stated above. Note that the results from the last two methods are similar or slightly better than the recommended methods.

Although the performance of the methods using the theorem in this paper is encouraging, there are still a lot of things we may want to know before we can recommend such methods with confidence. For instance, we may ask questions on stability. Are the methods obtained generally stable? If not, to what class do we limit our problem to obtain stability? How about higher order methods? We hope these questions can be answered to further simplify the use of Runge-Kutta methods.

REFERENCES

[1] Cohen, A.M., et al. 1973. Numerical Analysis. McGraw-Hill, London. pp. 213-216.

[2] Lagare, M.E. 1987a. Improper Riemann integrals and uniformly regular matrices. *SEA Bull. Math.* 11(1):23-26.

[3] Lagare, E.M. 1987b. *Matrices and the numerical integration of some classes of Henstock integrable functions.* Ph.D. Dissertation. Ateneo de Manila University, Quezon City. pp. 15-22.

[4] Lagare, E.M. 1988. The generalized Riemann integral, uniformly regular matrices, and numerical integration. *Proc. of the Fourth Franco-SEAMS Joint Conference.* Chiang Mai University, Chiang Mai, Thailand. p. 327-344.

[5] Lee, P.Y. 1984. An approach to improper integrals. *Matimyas Matimatika* 8(3):20-23.

[6] Ralston, A., and P. Rabinowitz. 1978. A First Course in Numerical Analysis, International Edition. McGraw-Hill, Singapore, pp. 208-218.

A STUDY OF THE ELECTRON-TRANSFER REACTION OF *bis-(N,N'*-DIBENZYL-THIOUREA) DICHLOROCOBALT (II) AND *bis-(N,N'*-DIBENZYL-THIOUREA) DIBROMOCOBALT (II) IN NONAQUEOUS SOLUTIONS WITH HEXACYANOFERRATE (III)

LUZVISMINDA U. RIVERO, and GRACE I. PRADO
Ateneo de Davao University
8000 Davao City

ABSTRACT

The electronic absorption spectra of the solutions of *bis-(N,N'*-dibenzylthiourea)-dichlorocobalt(II), $[Co(dibenztu)_2Cl_2]$, and *bis-(N,N'*-dibenzylthiourea)dibromocobalt(II), $[Co(dibenztu)_2Br_2]$ in acetone, acetonitrile, and ethanol were measured. Aqueous K_3 $[Fe(CN)_6]$ was added in measured amounts to each of the solutions. The absorption spectra were measured at definite time intervals to monitor changes in the absorption peaks. The formation of a bridged intermediate for the transfer of electron from the cobalt (II) moiety to $[Fe(CN)_6]^{3-}$, similar to those reported in the literature for other cobalt (II) complexes, was evident. The change with time in the absorbance at the maximum wavelength of the intermediate was measured to determine the rate of formation and decomposition of the bridged complex.

The capability of the cobalt(III)- cobalt (II) system when stabilized by organic ligands, to transport oxygen molecule analogous to the Fe (III) – Fe (II) system in hemoglobin has aroused the interest of quite a number of researchers. The role of the cobalt (III) – cobalt (II) couple in catalyzing reactions has also been studied especially in biochemical reactions (1-7). The kinetics of the reduction of cobalt (III) has been the subject of many studies (8-19, 26-32) the studies cited focusing on the determination of the order of reaction in the formation of a bridged intermediate, with the subsequent decomposition. This study approaches the Co(III)-Co(II) equilibrium from the reversed direction, i.e., the spectroscopic study of cobalt(II)-cobalt(III) system in nonaqueous solution. The starting complex, *bis-(N,N'*-dibenzylthiourea)dichlorocobalt(II), hitherto referred to as $[Co(dibenztu)_2Cl_2]$, and *bis-(N,N'*-dibenzylthiourea)dibromocobalt(II), hitherto referred to as $[Co(dibenztu)_2Br_2]$ are pseudotetrahedral complexes. The previous studies so far started on octahedral cobalt (III) complexes. The spectroscopic properties of the

test complexes were reported earlier (20-21); and the reaction of the diphenylthiourea analog [(Co(diphentu)$_2$,Cl_2] with solid oxidizing agents was the subject of a previous study (22). The changes in the spectroscopic properties of solutions of the complexes in acetone, acetonitrile, and ethanol are reported here along with initial attempts to study the rates of the decomposition of the bridged intermediate.

EXPERIMENTAL

Materials. *N,N'*-dibenzylthiourea was prepared following the standard procedure of preparing thiourea derivatives (23). 46.8 mL of benzylamine, 40.0 mL of carbon disulfide and 63.5 mL 5% ethanol were cautiously mixed in a 500-mL round bottom flask provided with an efficient double surface condenser. The apparatus was set up in a hood. An absorption device containing 1 M $CuSO_4$ and 6 M HCl was attached to the top of the condenser to absorb the H_2S which was evolved. The solution of benzylamine and CS_2 in ethanol was refluxed for eight hours, then the excess CS_2 and ethanol was distilled off. The residue was washed with excess 1:10 HCl to remove the unreacted benzylamine, filtered, washed with distilled water and drained well. The crystals were dried at 80°C in the oven. Further purification was done by dissolving the crystals with minimum hot ethanol, under reflux. The solution was filtered while hot. The filtrate was cooled in ice water. The needle-like crystals were filtered, washed with hot water, and dried in the oven at 80°C. The crystals were stored in an amber bottle.

The complexes were prepared by mixing a solution of cobalt chloride/cobalt bromide in anhydrous ethanol with a solution of *N,N'*-dibenzylthiourea in anhydrous dichloroethane in a molar ratio 1 cobalt salt to 2 of dibenzylthiourea. Equal volumes of the solution were used. The resulting mixture was heated in a steam bath under reflux. Then the solution was concentrated in a rotary evaporator until crystals appeared which were then filtered off and dried between filter papers. The crystallization was done with dichloroethane.

Analytical grade $K_3[Fe(CN)_6]$ crystals were used to prepare the 0.001 M aqueous solution.

Apparatus. The melting points of the complexes were measured using the Beckman melting point apparatus. The Perkin-Elmer model 710 A IR spectrophotometer was used to measure the infrared spectra of the ligand and the complexes. The electronic absorption spectra were measured using the Pye-Unicam SP8-100 digital double beam UV-visible spectrophotometer from 200 to 800 nm. For each measurement, the reference used was the corresponding solvent.

Spectra of the Reacting Solutions. 3.00 mL of 0.001 M [Co(dibenztu)$_2$, Cl_2]/[Co(dibenztu)$_2Br_2$] in the corresponding solvent, was placed in the cuvette. 0.04 mL of the oxidizing agent was added, the mixture shaken, and the spectrum was scanned from 200-800 nm immediately after mixing. Then an additional 0.04 mL was added, followed by scanning within the time allowed. The procedure was repeated with an additional 0.04 mL of the oxidizing agent.

Kinetic Studies. The spectrophotometer was set at 390 nm for the measurement of change of absorbance with time. 3.00 mL of 0.001 M [Co(dibenztu)$_2$Cl$_2$] in acetone was placed in the cuvette. 0.04 mL of the oxidizing agent was added, followed by shaking. The absorbance of the solution was measured every ten seconds.

RESULTS AND DISCUSSION

Absorption Spectra of the Complexes in the Region 200-800 nm. The absorption spectra of [Co(dibenztu)$_2$ Cl$_2$] and [Co(dibenztu)$_2$Br$_2$] in acetone, in acetonitrile, and in ethanol in the region 200 to 800 nm are typical of a pseudoetrahedral [CoL$_2$X$_2$] complex. These spectra are shown in Figures 1 and 2 for [Co(dibenztu)2 Cl$_2$] and [Co(dibenztu)$_2$, Br$_2$] respectively. The absorption band at 600-690 nm is typical $^4A_2(F) \rightarrow {}^4T_1(P)$ transition corresponding to the $e^4t^3 \rightarrow e^3t^4$. The peak at 330 nm for the acetone and for the acetonitrile solutions, and at 280 nm for the ethanol solution, is a halide to metal charge-transfer band. The shift to shorter wavelengths for the ethanol solution is expected due to the increasing polarity of the solvent.

The organic ligand, *N,N'*-dibenzylthiourea, has a very intense absorption band at 230-235 nm, characteristic of the $\pi \rightarrow \pi^*$ transition in the aromatic ring. A weaker band is expected at about 280 nm but this has disappeared because of (a) the substitution in the benzene ring, (b) the solvent used, and (c) the dilution. The intense aromatic band at about 230 nm was affected by the solvent used. In Fig. 1, with acetone as the solvent, the absorbance for a 0.001 M solution of the ligand is 1.2 and this was only sightly changed upon coordination with cobalt (II) in both chloride and bromide complexes (Fig. 2). With a slightly more polar solvent, acetonitrile, the absorbance for the same concentration went up to ~ 2.5 and the peak was shifted slightly to 235 nm, but on coordination was shifted even more (240 nm for [Co(dibenztu)$_2$Cl$_2$) and 300 nm for [Co(dibenztu)$_2$Br$_2$]). The general appearance of this aromatic band also changed when the ligand bonded with Co(II). The intense peak was split and a shoulder appeared at 240 nm. This means that the bonding of the C = S to the metal ion has affected the π-system of the aromatic ring. This effect however, was exhibited only for acetonitrile as solvent. With a more polar solvent such as ethanol, the band returned to its original shape similar to that of the pure ligand in the case of [Co(dibenztu)$_2$Br$_2$]. For [Co(dibenztu)$_2$Cl$_2$], coordination has decreased the intensity of the band drastically.

As expected, the absorption bands were shifted slightly to longer wavelengths when the halide was changed from chloride to bromide. This shift was more pronounced in the UV region. The splitting and general appearance of the band at 575-685 nm were more affected by a change in halide ion and in solvent. [Co(dibenztu)$_2$Br$_2$] gave a more intense band, almost double that of the chloride analog. The intensity of this band in a tetrahedral cobalt (II) is due to the lack of symmetry of the tetrahedral configuration so that the *d* orbitals mix with *p* orbitals

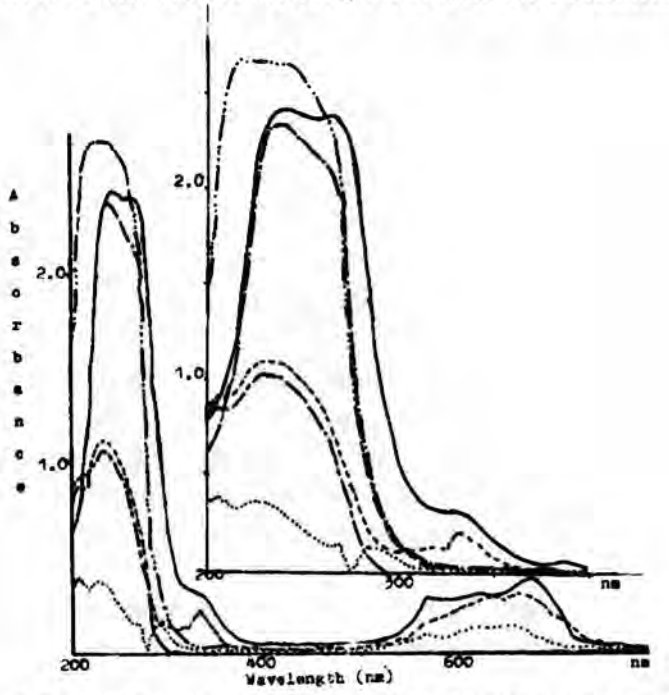

Figure 1. **The UV-visible absorption spectra of $[Co(dibenztu)_2Cl_2]$ in acetonitrile (——), in acetone (– – – –), in ethanol (· · · · ·), of dibenzylthiourea in acetonitrile (—— · ——) , in acetone (– —— –), in ethanol (—— · · ·).**

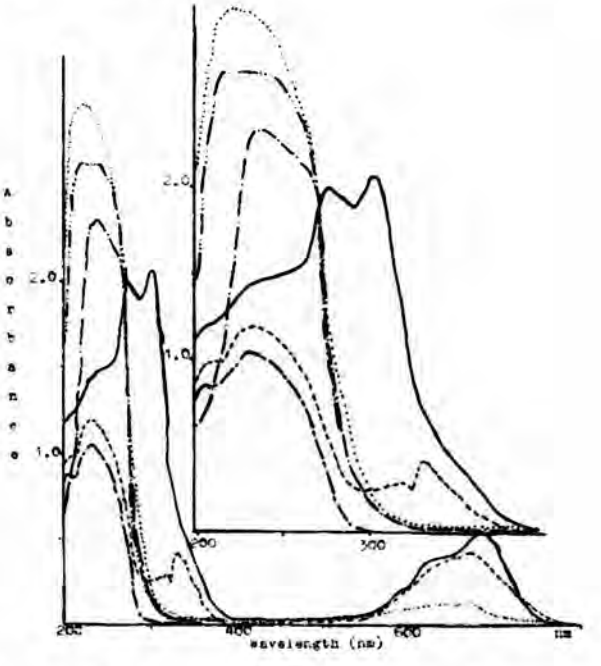

Figure 2. The UV-visible absorption spectra of $[Co(dibenztu)_2Br_2]$ in acetonitrile (——), in acetone (– – – –), in ethanol (· · · · ·), of dibenzylthiourea in acetonitrile (—— · ——) , in acetone (—— – ——), in ethanol (—— · · ·).

(same parity) hence no longer pure d orbitals, resulting in the lifting of Laporte's rule forbidding pure $d \longrightarrow d$ transitions. Bromide being a larger ion, allows more "mixing" of its *p*-orbitals with the *d*-orbitals of the central metal ion.

The splitting of the absorption band in the 575-685 nm region is due to spin-orbital coupling of the $^4P(T_1)$ state. $[CoCl_4]^{2-}$ for example, exhibits an unusually detailed splitting into five or six maxima (24). The lack of symmetry of the terahedral complex is the reason why spin-orbital coupling is more pronounced. The splitting of the $d \longrightarrow d$ transition band of $[Co(dibenztu)_2\ Cl_2]$ is more pronounced than that of $[Co(dibenztu)_2Br_2]$ complex. The solvents can also obscure this finer structure of the absorption band. Less polar solvents like acetone practically "dampen" this splitting. More polar solvents like ethanol, allow this splitting to be measured, especially in the total absence of water molecules. In Figure 3, the splitting is clearest for $[Co(dibenztu)_2Cl_2]$ in acetonitrile.

The absorption band of the solutions of the two complexes and of the pure ligand in acetone, in acetonitrile, and in ethanol, in the region 200-800 nm, are summarized in Table 1, along with the assignment of the transitions responsible for the absorption.

Oxidation with $[Fe(CN_6]^{3-}$. The reduction of $[Fe(CN_6]^{3-}$ to $[Fe(CN_6]^{4-}$ by $[Co(NH_3)_6]^{2+}$ is thermodynamically favorable in aqueous solution, the net reaction having a standard emf of 0.26 v at 25°C. With a change of ligand and coordination on cobalt (II) it is expected that the reaction will still be spontaneous.

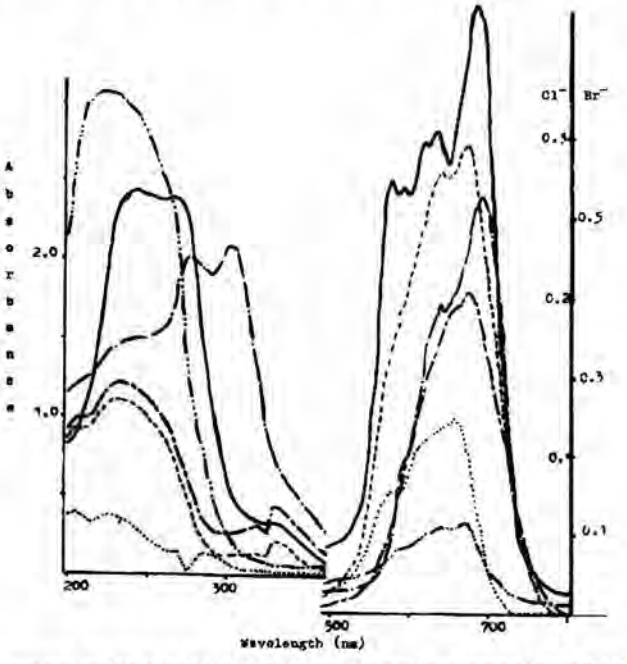

Figure 3. Comparison of the UV-Visible absorption spectra of $[Co(dibenztu)_2Cl_2]$ in acetonitrile (——), in acetone (– – – –), in ethanol (· · · · ·), of [Co)dibenztu)$_2Br_2$] in acetonitrile(—— · ——) , in acetone (– —— –), in ethanol (—— · · · ——).

Table 1. The maxima of the UV-visible spectra of dibenzylthiourea(dibenztu), $[Co(dibentzu)_2Cl_2]$ and $[Co(dibenztu)_2Br_2]$ in the three solvents with the corresponding molar extinction (liter per mole per cm) and assigned transitions.

	Wavelength (molar absorptivity)			
Solvent	Dibenztu	$[Co(Dibentzu)_2Cl_2]$	$[Co(Dibenztu)_2Br_2]$	Assignment
Acetone		670(296)	670(404)	$^4A_2(F) \rightarrow$
		640(278)		$^4T_1(P)$
		585(179)		
		330(227)	330(409)	X^- to
				Me, CT
	230(1045)	230(1110)	235(1197)	aromatic
	205(865)	205(924)		$\pi \rightarrow \pi^*$
Acetonit-		630(384)	685(524)	$^4A_2(F) \rightarrow$
rile		630(305)	635(389)	$^4T_1(P)$
		575(273)	590(186)	
		335(308)	355(350)	X^- to
	235(2357)	265(2392)	300(2059)	Me, CT
		240(2422)	275(2003)	aromatic
			240(1465)	$\pi \rightarrow \pi^*$
Ethanol		655(123)	670(111)	$^4A_2(F)$
			640(106)	$^4T_1(P)$
		580(76)	580(74)	
		285(144)	265(2292)	X^- to Me, CT
	230(2672)	230(375)	225(3023)	aromatic
		205(389)		$\pi \rightarrow \pi^*$

A change of solvent however, will slow down the reaction such that it is possible to monitor the change spectrophotometrically especially if one of the reagents is added in very limited amounts. In this study hexacyanoferrate (III) was added to $[Co(dibenztu)_2Cl_2]$ and to $[Co(dibenztu)_2Br_2]$ in measured amounts but the molar ratio was limited to 1 $[Fe(CN^6]^{3-}$ to 225 Co(II), then 1:112.5, then 1:75. Following the mechanism reported by previous researchers (16, 19, 26-31) the reaction is thought to proceed via the mechanism

$$[Fe^{III}(CN^6]^{3-} + [Co^{II}(Dibenztu)_2\,Cl_2] \longrightarrow [(NC)_5Fe^{III}\text{–}CN\text{–}(Co^{II}(Dibenztu)_2\,Cl_2]^{3-}$$

$$[(NC)_5Fe^{III}\text{–}CN\text{–}(Co^{II}(Dibenztu)_2\,Cl_2]^{3-} \longrightarrow [(NC)_5Fe^{II}\text{–}CN\text{–}(Co^{III}(Dibenztu)_2\,Cl_2]^{3-}$$

$$\mathbf{[(NC)_5Fe^{II}\text{–}CN\text{–}(Co^{III}(Dibenztu)_2\,Cl_2]^{3-} \longrightarrow [Fe^{II}(CN_6]^{4-} + Co^{III}\ products}$$

The changes in the spectra of the complexes upon the addition of $[Fe(CN_6]^{3-}$ are shown in Figures 4 to 8. With increasing amount of reagent, the intensity of the absorption band at ~ 670 nm decreased proportionately. The intensity of the new band at ~ 390 nm increased with the amount of reagent. If the millimoles of $[Co(dibenztu)_2Cl_2]$ left in the solution after each addition of reagent is subtracted from the original millimoles of complex, the millimoles of Co(III), bridged with $[Fe(CN_6]^{3-}$ can be estimated. The results are given in Table 2.

In Table 2, one notices immediately that the more polar the solvent, the more of the divalent complex has been converted to Co(II). The obvious trend that the more reagent added, the more Co(II) complex is oxidized, is affirmed. Only in the less polar solvents acetone and acetonitrile, is the trend 1:2:3, following the mmoles of reagent added, is approximated, but only for $[Co(Dibenztu)_2Cl_2]$. The bromide is "helping" the $[Fe(CN)_6]^{3-}$ so to speak, in oxidizing the Co(II) central atom. The absolute mmoles of oxidized complex however, exceed the mmoles of $[Fe(CN)_6]^{3-}$ added, as shown in Table 3. The ratio of conversion is biggest for ethanol, the trend decreasing with more reagent added. The opposite is true for weakly polar acetone as solvent. The ratio of conversion is smallest and the trend is increasing. The increase in conversion ratio is not as much in acetonirile compared to acetone. In some cases in fact, the ratio decreases. Again, the polarity of the solvent plays a role in the reaction.

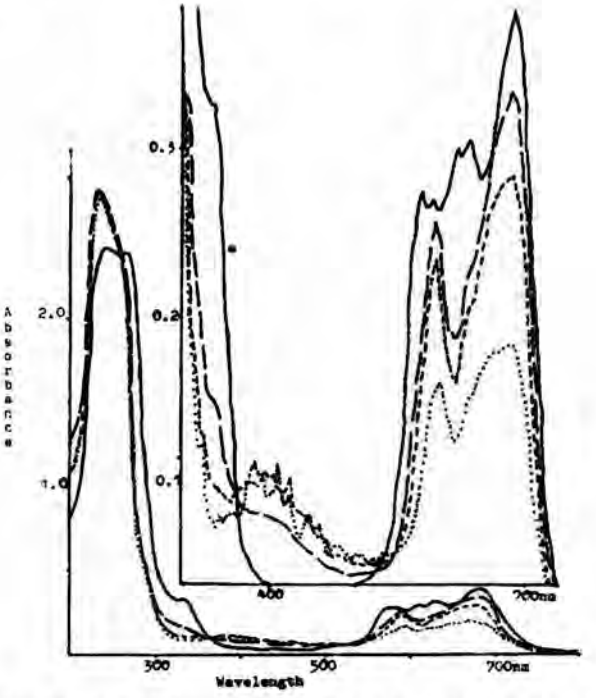

Figure 4. The absorption spectrum of $[Co(dibenztu)_2Cl_2]$ acetonitrile (0.001 M (——), upon addition of 0.001 M K_3 $[Fe(CN)_6]$ to 3.0 mL of complex, 0.04 mL (———), 0.08 mL (– – – –), 0.12 mL (· · · · ·). The inset is a magnified absorption spectrum in the visible region..

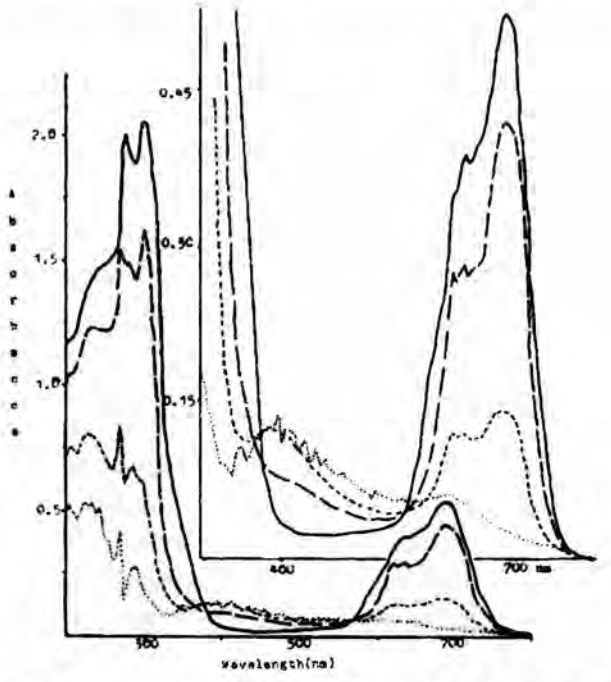

Figure 5. The absorption spectrum of $[Co(dibenztu)_2Br_2]$ acetonitrile (0.001 M (——), upon addition of 0.001 M K_3 $[Fe(CN)_6]$ to 3.0 mL of complex, 0.04 mL (—— ——), 0.08 mL (– – – –), 0.12 mL (· · · · ·). The inset is a magnified absorption spectrum in the visible region..

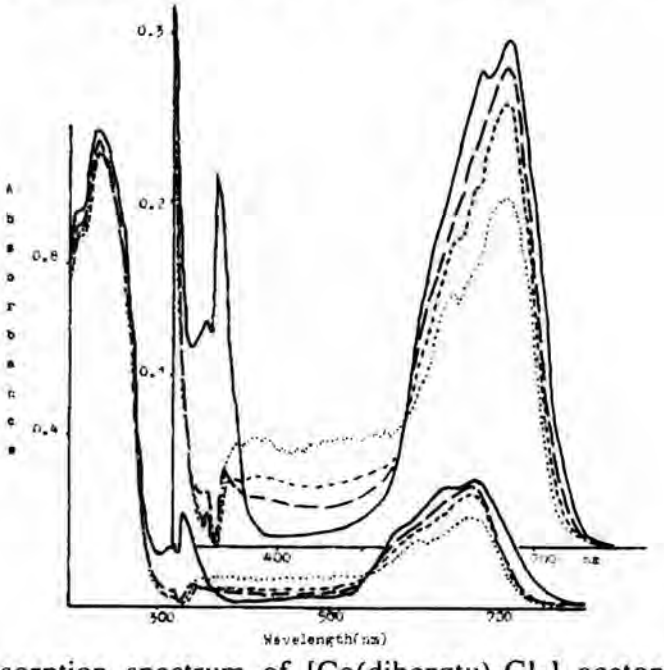

Figure 6. The absorption spectrum of $[Co(dibenztu)_2Cl_2]$ acetone (0.001 M (——), upon addition of 0.001 M K_3 $[Fe(CN)_6]$ to 3.0 mL of complex, 0.04 mL (—— ——), 0.08 mL (– – – –), 0.12 mL (· · · · ·). The inset is a magnified absorption spectrum in the visible region.

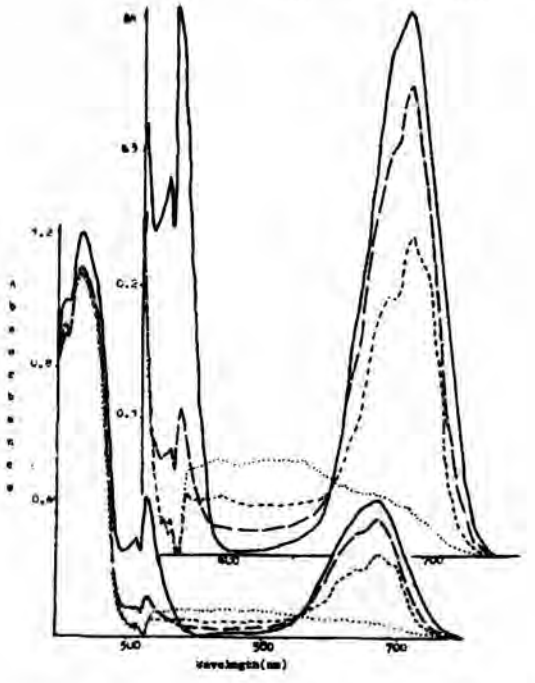

Figure 7. The absorption spectrum of $[Co(dibenztu)_2Br_2]$ acetone (0.001 M (——), upon addition of 0.001 M K_3 $[Fe(CN)_6]$ to 3.0 mL of complex, 0.04 mL (—— ——), 0.08 mL (––––), 0.12 mL (· · · · ·). The inset is a magnified absorption spectrum in the visible region..

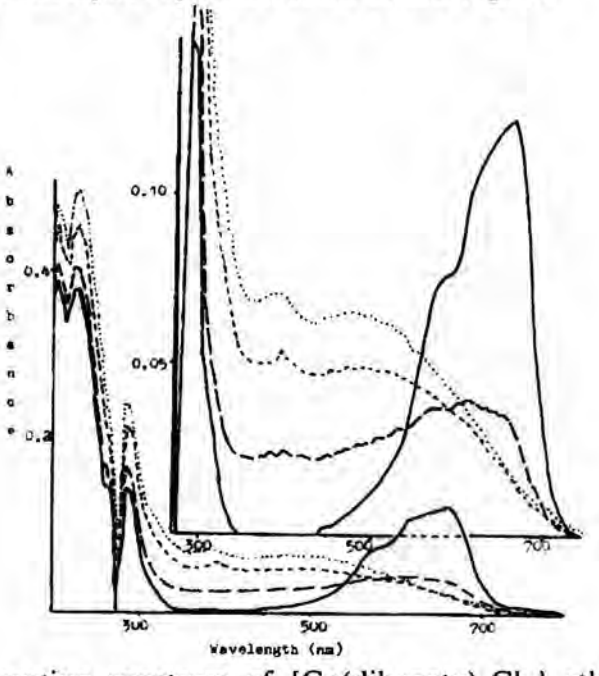

Figure 8. The absorption spectrum of $[Co(dibenztu)_2Cl_2]$ ethanol (0.001 M (——); upon addition of 0.001 M K_3 $[Fe(CN)_6]$ to 3.0 mL of complex, 0.04 mL (—— ——), 0.08 mL (––––), 0.12 mL (· · · · ·). The inset is a magnified absorption spectrum in the visible region..

Table 2. Millimoles (x103) Co(II) complex converted to Co(III), obtained from the decrease in absorbance of Co(II) complex after addition of 0.001 M $K_3[Fe(CN)_6]$

Solvent	$[Co(dibentzu)_2Cl_2]$			$[Co(dibenztu)_2Br_2]$		
	0.04 mL	0.08 mL	0.12 mL	0.04 mL	0.08 mL	0.12 mL
Acetone	1.12	2.9	8.47	3.89	12.04	27.23
Acetonitrile	4.5	7.2	15.3	5.6	21.68	26.41
Ethanol	20.03	24.7	24.88	21.91	22.92	23.48

Table 3. Ratio of mmoles of Co(II) complex converted to Co(III) to the mmoles of $[Fe(CN)_6]^{3-}$ added to 3.00 mL of 0.001 M complex

Solvent	$[Co(dibentzu)_2Cl_2]$			$[Co(dibenztu)_2Br_2]$		
	0.04 mL	0.08 mL	0.12 mL	0.04 mL	0.08 mL	0.12 mL
Acetone	2.8	3.6	7.0	9.7	15.0	22.7
Acetonitrile	11.2	9.0	12.8	14.0	27.1	22.0
Ethanol	50.1	30.9	20.8	54.8	28.6	19.6

Both $[Co(dibenztu)_2Cl_2]$ and $[Co(dibenztu)_2Br_2]$ show the absorption band at 360-380 nm, which is characteristic of the bridge Co(III) ion, attributed to the $^1A_1g \rightarrow {}^1T_{2g}$ transition.

With ethanol as solvent, the bridge intermediate is detectable from the hump at around 500 nm, and the peak at 376 nm, both for the chloride and bromide complexes (Figures 8 and 9). Such a hump is discernible in the acetone solution of both complexes with the difference that the $d \rightarrow d$ transition band with increasing spin-orbital coupling is still intact, albeit reduced in intensity (Figures 6 and 7). This band practically disappeared in the ethanol solution upon the addition of 0.12 mL 0.001 M $K_3[Fe(CN)_6]$.

The acetonitrile solution of each of the complex retained the absorption band at ~ 680 nm (Figures 4 and 5) but with reduced spin-orbital splitting. The intensity of the band was reduced. The absorption band at 388 nm increased in intensity, with the formation of many peaks on third addition of the reagent. The reason for these peaks is not clear at the moment, although this can be a sign of a decrease in symmetry such that spin-orbital coupling has increased.

The specific wavelengths of the absorption band for Co(III) for the transition $^1A_{1g} \rightarrow {}^1T_{2g}$ are given in Table 4, along with the corresponding molar absorptivity. The assignment of this band is based on the spectra of Co(III) complexes reported in other studies (3, 16, 25) and also in the assignment of transitions in d^6 tetrahedral complexes as discussed by Schlaefer and Gliemann (24).

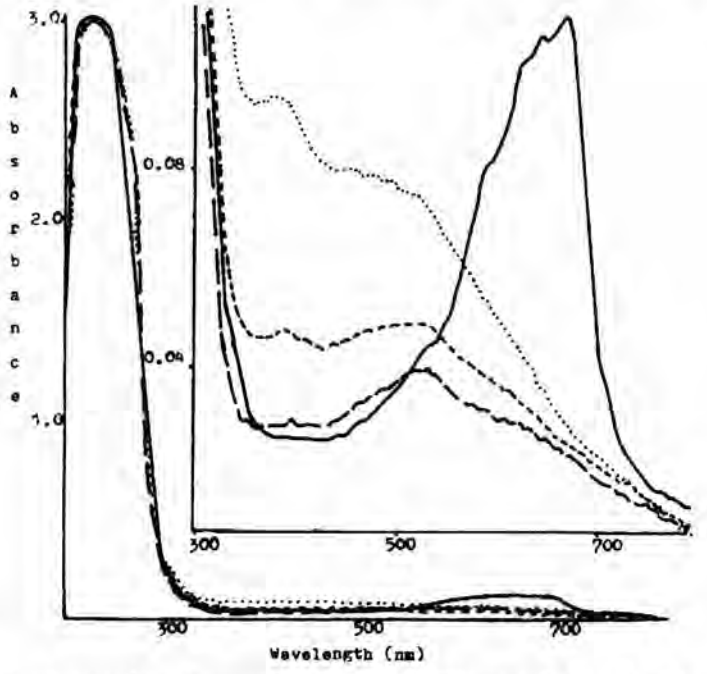

Figure 9. The absorption spectrum of $[Co(dibenztu)_2Br_2]$ ethanol (0.001 M (——), upon addition of 0.001 M $K_3[Fe(CN)_6]$ to 3.0 mL of complex, 0.04 mL (— — —), 0.08 mL (– – – –), 0.12 mL (· · · · ·). The inset is a magnified absorption spectrum in the visible region..

Table4. The new absorption band which appeared upon the addition of 0.12 mL, 0.001M $K_3[Fe(CN)_6]$ to 3.0 mL of 0.001 M solution of complex in the corresponding solvent.

	Wavelength, nm (molar absorptivity)	
Solvent	*$[Co(Dibentzu)_2Cl_2]$*	*$[Co(Dibenztu)_2Br_2]$*
Acetone	372(68)	372(70)
Acetonitrile	388(112)	388(132)
Ethanol	384(70)	376(95)
	476(65)	456(80)

It is to be noted that the molar absorptivities of the intermediate of the bromide complexes were higher than those of chloride analog. Furthermore, the absorption band for the ethanolic solution was shifted to higher wavelengths for the bromide complex, compared to the corresponding bands for $[Co(dibenztu)_2Cl_2]$.

Another interesting change in the absorption spectra of $[Co(dibenztu)_2Cl_2]$ and $[Co(dibenztu)_2Br_2]$ in the three solvents is the behavior of the halide to metal

charge transfer band at around 300 nm upon the addition if $[Fe(CN)_6]^{3-}$. The changes are summarized in Table 5.

The charge-transfer band of the complex is intensified by the polarity of the solvent. Upon addition of the oxidant, the charge-transfer even increases in intensity, along with the aromatic band, if the solvent is polar. This is detectable in the ethanolic solution of $[Co(dibenztu)_2Cl_2]$ and $[Co(dibenztu)_2Cl_2]$. This can mean that the transfer of the electron affects the chloride. This is understandable from the configuration of the complex. The approach of the $[Fe(CN)_6]^{3-}$ can only be through the side of the halide ligands since the other side is blocked by the bulky dibenzylthiourea ligands, as the following illustration shows:

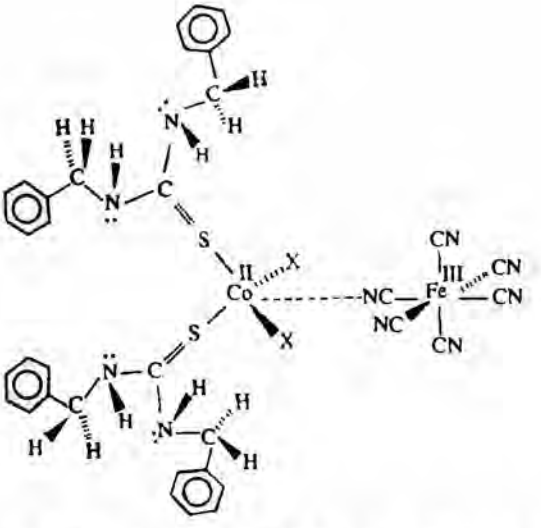

The Formation and Decomposition of a Reaction Intermediate. The formation of a cyanide-bridged intermediate between $[CoCyDTA]^{2-}$ and $[Fe(CN)_6]^{3-}$ has been reported by Huchital and Hodges (26) to be the path of the following reaction:

$$[CoY]^{2-} + [Fe(CN)_6]^{3-} \rightleftarrows [Y - Co^{III} - CN - Fe^{II}(CN)_5]^{5-} \xrightarrow{k_3}$$

$$[Co\,Y]^{-} + [Fe(CN)_6]^{4-}$$

Where Y stands for 1,2 –cyclohexanediamine tetraacetate. In later reports, Huchital and Lepore (27) and Rosenheim, Speiser, and Haim (19) had shown that the reduction of hexacyanoferrate(III) ion $[Fe(CN)_6]^{3-}$ by ethylenediaminetetraacetatocobaltate(II), $[CoEDTA]^{2-}$ proceed via the following mechanism:

$$[Fe^{III}(CN)_6]^{3-} + [Co^{II}(EDTA]^{2-} \underset{k_{-1}}{\overset{k_1}{\rightleftarrows}} [(NC)_5Fe^{III} - CN - Co^{II}(EDTA]^{5-}$$

$$k_{-e.t.} \uparrow\downarrow k_{\text{electron transfer}}$$

$$[(NC)_5Fe^{II} - CN - Co^{III}(EDTA]^{5-}$$

$$k_{-3} \uparrow\downarrow k_3$$

$$[Fe^{II}(CN)_6]^{4-} + [Co^{III}(EDTA]^{2}$$

Table 5. Changes of the halide → metal charge-transfer band upon the addition of oxidant to the solution.

Charge-transfer band present in original complex		Charge transfer-band not present in original complex nor upon addition
Disappeared upon addition of reagent	Still present/ increased upon addition of reagent	
$[Co(dibenztu)_2Cl_2]$ in acetone		
$[Co(dibenztu)_2Br_2]$ in acetone		
$[Co(dibenztu)_2Cl_2]$ in acetonitrile		
	$[Co(dibenztu)_2Br_2]$ in acetonitrile	
	$[Co(dibenztu)_2Br_2]$ in ethanol	$[Co(dibenztu)_2Br_2]$ in ethanol

The bridged intermediate, [L-Fe(III)-CN-Co(III)-L], can be made stable depending on the other ligands in Co(III). Reagor et al. (16) reported that with *N*-hydroxyethylEDTA and *N*-benzylEDTA, the binuclear bridged species can be stored at room temperature indefinitely without detectable decomposition.

The studies just mentioned were carried out in aqueous solutions. In the present study which is carried out in nonaqueous solvents, the existence of the bridged intermediate in reactions of tetrahedral Co(II) complexes with $[Fe(CN)_6]^{3-}$ is evident from the appearance of new absorption bands. The change of absorbance of the solution of the complex upon addition of the reagent was added, was monitored.

There are three possible behaviors of the bridged intermediate: first, when at least one of the product ions is substitution labile, the decay of the successor binuclear complex is very rapid; second, the bridged complex decomposes slowly – this happens when an inner-sphere redox reaction, for example, occurs between two complexes in which both product metal centers are substitution inert and in addition, one of the metal ions is complexed with a multidentate ligand; third, both the product ions are substitution inert such that the cyano-bridged species can be extremely stable.

The stability of the intermediate found in this study appears to depend on the solvent used, and the partner ion in the complex. Kinetic studies were carried out by reacting 3.0 mL of 0.001 M $[Co(dibenztu)_2Cl_2]$ in acetonitrile and of $[Co(dibenztu)_2Cl_2]$ in acetone and in acetonitrile, with 0.04 mL, 0.08 mL, 0.12 mL of aqueous 0.001M $K_3[Fe(CN)_6]$ solution. Figure 10 shows the changes in the absorbance of the solutions of cobalt(II) complex plus the reagent at 390 nm. In most cases, the formation of an absorbing species is evident from the increase in absorbance; the decay of this species into a stable moiety is also evident from the decrease in absorbance.

The increase in absorbance when $[Co(dibenztu)_2Cl_2]$ in acetone reacted with 0.04 mL of the oxidant (Figure 10) indicates that formation of an intermediate spe-

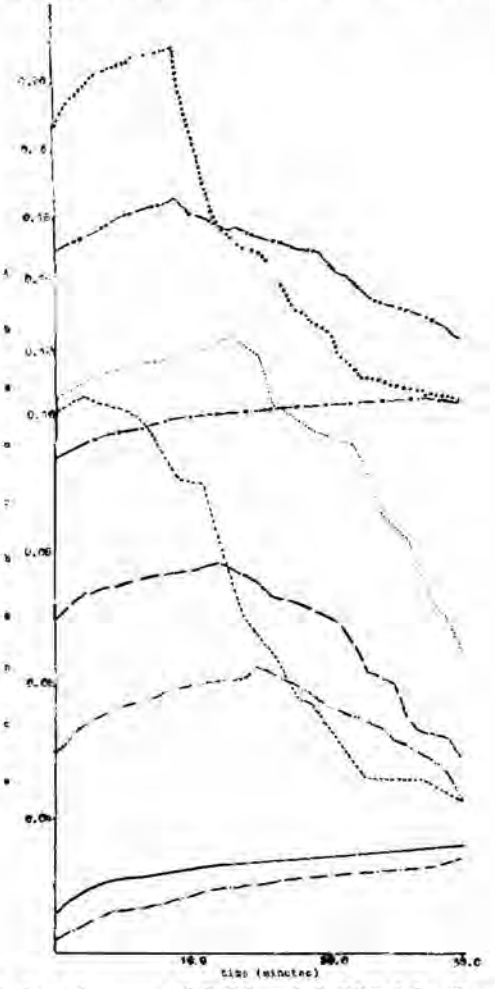

Figure 10. Change of absorbance of 3.00 ml 0.001 M of complex with time upon addition of 0.001 M $K_3[Fe(CN)_6]$: $[Co(dibenztu)_2Cl_2]$ in acetone, 0.04 mL oxidant (——), 0.08 mL (— — —), 0.12 mL (— — —), $[Co(dibenztu)_2Br_2]$ in acetone, 0.04 mL oxidant, (— . — .), 0.08 mL (— ... —), 0.12 mL (.....); $[Co(dibenztu)_2Cl_2]$ in acetonitrile, 0.04 mL oxidant (—·—·), (—··—··), 0.12 mL (·····).

cies is still going on at the time the absorbances were measured. However, upon addition of more reagent, the formation of the intermediate is completed earlier, at 12 and 2 min for 0.04 and 0.08 mL respectively and a subsequent decay of the intermediate species is observed.

As illustrated in Figure 10, an increase of absorbance occurred when $[Co(dibenztu)_2Br_2]$ in acetone reacted with 0.04 mL of the oxidant. When additional reagent was added, the times needed for the completion of the formation of the intermediate are 15 and 13 minutes for 0.08 and 0.12 mL respectively. These are longer compared to the reaction of the chloride analog in the same solvent.

It is to be noted that the decomposition of the intermediate appears to proceed in steps, as evident in the periodic humps of the absorbances of the solution to which 0.12 mL of the oxidant has been added. This will be the subject of a separate study later.

CALCULATION OF RATE CONSTANTS

All reactions were carried out under pseudo-first order conditions with Co(II) complexes in large excess over the oxidant, aqueous K_3 $[Fe(CN)_6]$, at room temperature. Reactions were observed at 390 nm. The log (A_t-A_∞) for the reaction $[Co(dibenztu)_2Cl_2]$ in acetonitrile and 0.08 mL of aqueous K_3 $[Fe(CN)_6]$ where A_t and A_∞ are the absorbances at time t and after 10 min after mixing respectively, are plotted vs time. Figures 11 and 12 show the resulting graph of the rate constants of

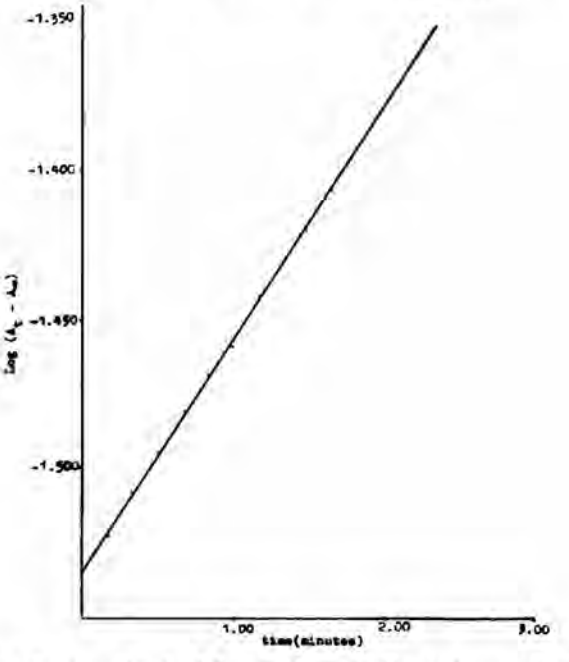

Figure 11. Apparent rate constant of formation of the intermediate, 3.00 mL 0.01 M $[Co(dibenztu)_2Cl_2]$ in acetonitrile plus 0.08 mL 0.001 M K_3 $[Fe(CN)_6]$. A_t is the absorbance at time t; A_∞ is the absorbance after 10 minutes.

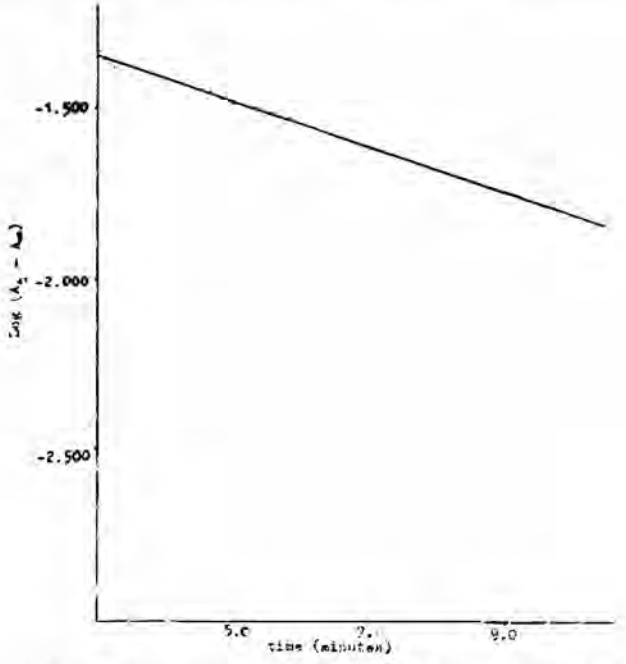

Figure 12. Apparent rate constant of formation of the intermediate, 3.00 mL 0.01 M $[Co(dibenztu)_2Cl_2]$ in acetonitrile plus 0.08 mL 0.001 M $K_3[Fe(CN)_6]$. A_t is the absorbance at time t; A_∞ is the absorbance after 10 minutes.

formation and of decomposition of an intermediate species, respectively. The rate constants were determined as the linear slopes of plots of log (A_t-A_∞) vs time. Based on the plots, the apparent rate constant of intermediate formation (Figure 11) is $7.81 \times 10^{-2} min^{-1}$ or 1.3×10^{-3} sec^{-1}. The apparent rate constant of intermediate decomposition is 1.72×10^{-2} min^{-1} or 2.87×10^{-4} sec^{-1}.

Thus the reaction of $[Co(dibenztu)_2Cl_2]$ and of $[Co(dibenztu)_2Br_2]$ solutions in acetone, in acetonitrile, and in ethanol, with the aqueous oxidant $K_3[Fe(CN)_6]$ involves an inner-sphere mechanism of electron transfer as evident in the formation of a bridged intermediate.

REFERENCES

1. C.R. Clark, R.F. Tasker, D.A. Buckingham, D.R. Knigator, D.R.K. Harding, and W.S. Haniochi. 1981. *Journal of the American Chemical Society* 103:7023.
2. L.S. Hegedus and Y.Inone. 1982. *Journal of the American Chemical Society* 104:4917.
3. H. Sakarai, 1982. *Journal of the American Chemical Society* 104:4960.
4. S.S. Isied, A. Vassilia, and J.M. Lyn. 1982. *Journal of the American Chemical Society* 104:3910.
5. N. Saha and H. Sigel. 1982. *Journal of the American Chemical Society* 104:4100.

6. S. Larsson 1981. *Journal of the American Chemical Society* 103:4034.
7. E.D. Stevens. 1981. *Journal of the American Chemical Society* 103:5087.
8. A.P. Szecsy and A. Haim. 1982. *Journal of the American Chemical Society* 104:3063.
9. H. Price and H. Taube. 1968. *Inorganic Chemistry* 7(1):1.
10. D. Gaswick and A. Haim. 1974. *Journal of the American Chemical Society* 96:7845.
11. P. Siders and R.A. Marcus. 1981. *Journal of the American Chemical Society* 103:741.
12. D.H. Huchital and R.G. Wilkins. 1967. *Inorganic Chemistry* 6:1022.
13. K. Wieghardt and H. Spiecker. 1977. *Inorganic Chemistry* 16(6): 1290.
14. S.K.S. Zawacky and H.Taube. 1981. *Journal of the American Chemical Society* 103:3379.
15. E.S. Gould. 1972. *Journal of the American Chemical Society* 94:4360.
16. B.T. Reagor, D.F. Kelley, D.H. Huchital, and P.M. Rentzepis. 1982. *Journal of the American Chemical Society* 104:7400.
17. J. Jwo, P.L. Gaus, and A. Haim. 1979. *Journal of the American Chemical Society* 101:6189.
18. P.R. Guenther and R.G. Linck. 1969. *Journal of the American Chemical Society* 91:3769.
19. L. Rosenheim, D. Speiser, and A. Haim. 1974. *Inorganic Chemistry* 13(7):1571
20. A. Quimsing and L.U. Rivero. 1984. *Agham* 10(3):121.
21. A. Quimsing, and L.U.Rivero. 1983. *Agham* 10(2):75.
22. L.U. Rivero and C. Ballesil. 1984. *Trans. Nat. Acad. Science & Tech.* 6:87.
23. A.I. Vogel. 1956. "A Textbook of Practical Organic Chemistry Including Organic Analysis".
24. H.L. Schlaefer and G. Gliemann. 1967. "Einfuehrung in die Ligandenfeldtheorie", Academische Verlagsgesellscaft, Frankfurt am Main, pp. 21, 54-55, 97, 101-102.
25. F.A. Cotton and G. Wilkinson. 1968. "Anorganische Chemie", 2. Auflage, translated by H.P. Fritz, Verlag Chemie GmbH., Weinheim/Bergstr., Germany, p. 817.
26. D.H. Huchital and R.J. Hodges. 1973. *Inorganic Chemistry* 12:998.
27. D.H. Huchital and J. Lepore. 1978. *Inorganic Chemistry* 17:1134.
28. H. Phillips and A. Haim. 1980. *Inorganic Chemistry* 19:1616.
29. C. Hwang and A. Haim. 1970. *Inorganic Chemistry* 9:500.
30. M. Hery and K. Wieghardt. 1978. *Inorganic Chemistry* 17(5):1130.
31. D.H. Huchital and R.J. Hodges. 1973. *Inorganic Chemistry* 12(5):1004.
32. F.F. Fan and E.S. Gould. 1974. *Inorganic Chemistry* 13(11): 2647.